ISPRS Journal of Photogrammetry and Remote Sensing 170 (2020) 156–173

Contents lists available at ScienceDirect

ISPRS Journal of Photogrammetry and Remote Sensing

journal homepage: www.elsevier.com/locate/isprsjprs

Characterizing spatiotemporal patterns of crop phenology across North America during 2000–2016 using satellite imagery and agricultural survey data

Yanjun Yang [a], Wei Ren [a,*], Bo Tao [a,*], Lei Ji [b], Liang Liang [c], Alex C. Ruane [d], Joshua B. Fisher [e], Jiangui Liu [f], Michael Sama [g], Zhe Li [h], Qingjiu Tian [i]

[a] Department of Plant and Soil Sciences, College of Agriculture, Food and Environment, University of Kentucky, KY 40546, USA
[b] ASRC Federal Data Solutions, Contractor to USGS EROS Center, Sioux Falls, SD 57198, USA
[c] Department of Geography, College of Arts & Sciences, University of Kentucky, KY 40506, USA
[d] NASA Goddard Institute for Space Studies, New York, NY, 10025, USA
[e] Jet Propulsion Laboratory, California Institute of Technology, Pasadena, CA 91109, USA
[f] Ottawa Research and Development Centre, Agriculture and Agri-Food Canada, Ottawa, ON K1A0C6, Canada
[g] Department of Biosystems and Agricultural Engineering, College of Agriculture, Food and Environment, University of Kentucky, KY 40546, USA
[h] Center for Space Research, University of Texas at Austin, Austin, TX 78759, USA
[i] International Institute for Earth System Science, Nanjing University, Nanjing 210023, China

ARTICLE INFO

Keywords:
North America
Crop phenology
Cropping intensity
Climate change
EVI-curve-based approach
Spatiotemporal trend analysis

ABSTRACT

Crop phenology represents an integrative indicator of climate change and plays a vital role in terrestrial carbon dynamics and sustainable agricultural development. However, spatiotemporal variations of crop phenology remain unclear at large scales. This knowledge gap has hindered our ability to realistically quantify the biogeochemical dynamics in agroecosystems, predict future climate, and make informed decisions for climate change mitigation and adaptation. In this study, we improved an EVI-curve-based approach and used it to detect spatiotemporal patterns in cropping intensity and five major phenological stages over North America during 2000–2016 using vegetation index in combination with agricultural survey data and other ancillary maps. Our predicted crop phenological stages showed strong linear relationships with the survey-based datasets, with R^2, RMSEs, and MAEs in the ranges of 0.35 –0.99, three to ten days, and two to eight days, respectively. During the study period, the planting dates were advanced by 0.60 days/year ($p < 0.01$), and harvesting dates were delayed by 0.78 days/year ($p < 0.01$) over North America. A minimum temperature increase by 1 °C caused a 4.26-day planting advance ($r = -0.50$, $p < 0.01$) or a 0.66-day harvest delay ($r = 0.10$, $p < 0.01$). While, a higher maximum temperature resulted in a planting advance by 4.48 days/°C ($r = -0.62$, $p < 0.01$) or a harvest advance by 2.22 days/°C ($r = -0.40$, $p < 0.01$). Our analysis illustrated evident spatiotemporal variations in crop phenology in response to climate change and management practices. The derived crop phenological datasets and cropping intensity maps can be used in regional climate assessments and in developing adaptation strategies.

1. Introduction

Vegetation phenology, defined as the development, differentiation, and initiation of plant organs (Hodges, 1991), is an integrative indicator of climate change (Badeck et al., 2004). Changes in vegetation phenology may have significant feedback to ecosystems and climate via the biogeochemical (e.g., CO_2 releases or uptakes) and biophysical processes (e.g., albedo) (Jin et al., 2013; Chen et al., 2015). Compared to natural vegetation phenology, crop phenology is more complicated. It is regulated by not only natural factors (e.g., climate) but also intensive management practices (e.g., cultivars and decisions on sowing dates) (Tao et al., 2012). Crop phenology usually exhibits multiple cycles in a season as a result of diverse cropping systems and multiple crop intensity (Li et al., 2014; Yan et al., 2014, 2019). Globally, agricultural fields occupy approximately 37.2% of the global ice-free land surface, in which approximately 32% is used for crop production (Ren et al., 2008).

* Corresponding authors.
E-mail addresses: wei.ren@uky.edu (W. Ren), bo.tao@uky.edu (B. Tao).

https://doi.org/10.1016/j.isprsjprs.2020.10.005
Received 4 December 2019; Received in revised form 20 September 2020; Accepted 8 October 2020
Available online 30 October 2020

Accurate information of crop phenology over large areas is crucial for advancing our understanding of agricultural ecosystem functioning and structure, monitoring crop growth, realistically estimating carbon dynamics, and developing viable management practices for climate adaptation and mitigation (Lobell et al., 2013; Diao, 2020; Mercier et al., 2020).

In the context of climate change, shifted crop phenology, such as the advanced planting dates and delayed harvesting dates, has been widely reported (Piao et al., 2006; Oteros et al., 2015; Sacks and Kucharik, 2011). Generally, crop phenology information was mainly obtained from field observations (Tao et al., 2006), remote sensing imagery (Xu et al., 2017), phenology modeling (Liu et al., 2013), and survey data (Portmann et al., 2010). However, limited site-level observations and district-based surveys (Sakamoto, et al., 2005) cannot fully capture highly variable patterns in crop phenological stages over large areas (Piao et al., 2019; Zhang et al., 2020). Moreover, phenology algorithms/models are usually fed by climate data such as temperature and soil moisture, without or with relatively much fewer considerations about land management and practices (Tveito et al., 2005; Wu et al., 2010). These limitations potentially bring large uncertainties to associated climate impacts and carbon balance assessments at broad scales.

With rapid development in remote sensing over past decades, satellite imagery with worldwide coverage and rapid re-visit times has made it possible to examine and monitor phenological variations over large areas (Pan et al., 2015; White et al., 2014; Zeng et al., 2016; Zhang et al., 2020). However, most crop phenology studies either constrained to a few specific crop types such as wheat, corn, soybean, and rice (Xin et al., 2002; Lu et al., 2013) or targeted on limited crop growing stages (e.g., the start or end of the season) (Liu et al., 2017a,b). Moreover, crop phenological stages (e.g., silking, denting, or maturity dates) in multiple cropping systems with a rotation of one or two crops per year have not been well addressed (Gumma et al., 2014). These knowledge gaps have hindered our ability to understand the role of crop phenology in food production, surface energy balance, and terrestrial biogeochemical cycles.

Over the recent decades, many methods have been developed to detect vegetation phenological events using vegetation indices (VI) time series (Liu et al., 2016b; Zhu et al., 2012; White et al., 2009). One of the essential processes of the satellite-based approach is to construct the VI time series using various filtering algorithms such as the Fourier filter (Roerink et al., 2000), the Savitzky-Golay filter (White et al., 2009), the asymmetric Gaussian function (Cong et al., 2012), double logistic function (Zhang et al., 2003), and the Whittaker smoother (Atkinson et al., 2012). Those functions can smooth out noise and fluctuations of the raw time series data, thus uncover the temporal patterns of crop phenological stages (Diao, 2020). Based on the constructed time series, crop phenological stages can be detected using various retrieval algorithms (e.g., inflection or transition point, changing rate, and threshold-defined methods) (Zhang et al., 2003; Wang et al., 2017).

The selection of the appropriate retrieval algorithms has substantial influences on estimated crop phenological stages (Gao et al., 2017; Diao, 2020). Of the numerous methods, threshold-based methods are often used because they generally keep dates within a specific reasonable range based on the threshold conditions and achieve relatively higher accuracy. For example, You et al. (2013) developed a threshold-based approach for identifying the start and end of the growing seasons for 43 different agricultural zones in China using the AVHRR satellite data and observed crop phenology at agro-meteorological stations. Although the threshold of each agricultural zone can be determined to produce reasonable estimates of crop phenological timing, it is very challenging to apply them directly over extended geographical regions, particularly for those without enough detailed ground observations. Combined with ground observations, Huang et al. (2019) demonstrated the importance of optimal thresholds for detecting crop phenological stages at the site-level by evaluating the retrieval accuracy of crop start and end seasons using different dynamic thresholds of VI time series. However, the site-level thresholds, to a large extent, cannot capture the regional or global crop seasonal patterns, which calls for a more systematic approach combining the advantages of the threshold-based method and characteristics of VI time series. This systematic approach should be able to fit seasonal and annual fluctuations of multiple phenological stages for major crop types at broader scales.

In this study, we used an EVI-curve-based approach for detecting spatiotemporal variations in the cropping intensity and five major crop phenological stages (i.e., the dates of planting, jointing, heading, maturity, and harvesting) of seven crop types over North America during 2000–2016. Our overarching scientific objectives are to (1) improve an EVI-curve-based approach for detecting changes in cropping intensity and dates of the five primary phenological stages at large scales; (2) generate spatially explicit crop rotation and phenology datasets over North America during 2000–2016; (3) characterize spatiotemporal variations of crop phenology and associated climatic driving factors; and (4) identify uncertainties and future research needs.

2. Materials and methods

2.1. Study area

The spatial domain in this study covers North America (includes Canada, the United States, and Mexico). Fertile soils, plentiful freshwater, and diverse climate all contribute to the agriculture development of North America, making it one of the most important crop production areas in the world. Its cultivated area occupies about 12.76% of the world's total acreage of cropland in 2016 (FAO, 2016) and covers more than 17% of the non-water, non-snow/ice areas of the entire continent (Reed, 2013). The U.S. alone produces 46% of the world's corn and 33% of the world's soybean, representing the largest corn and soybean producer (Taylor and Won, 2015). North America spans a range of latitudes and embraces diverse climates. Most of the continent has temperate climates favorable to agriculture. In this study, North American croplands (including annual crops, woody crops, and perennial crops and grasses) cover an area of 2,950,106 km^2.

2.2. Datasets

2.2.1. MODIS data

MODIS data have been widely used to monitor crop phenological changes (Thompson and Paull, 2017). In this study, crop phenological stages were retrieved for the continent of North America using MODIS EVI (Enhanced Vegetation Index) time series from February 2000 to December 2016. EVI was calculated using the valid NIR (Near Infrared Reflectance), red and blue band reflectance values from the land surface reflectance product MOD09A1 (version 6, ftp://ltdr.nascom.nasa.gov/allData). MOD09A1 provides 500-m and 8-day composite surface reflectance with seven bands in a Sinusoidal projection system, available from February 2000 through the present.

2.2.2. Cropland distribution data

The cropland distribution across North America was extracted from the 2005 and 2010 Land Cover Database of North America at a spatial resolution of 250 m (https://landcover.usgs.gov). This database was produced by the North American Land Change Monitoring System (NALCMS), a trilateral effort among the Canada Centre for Remote Sensing (CCRS), the United States Geological Survey (USGS), and three Mexican organizations, including the National Institute of Statistics and Geography, National Commission for the Knowledge and Use of the Biodiversity and the National Forestry Commission of Mexico. Cropland areas dominated by intensively managed crops include areas used to produce annual crops, such as corn, soybeans, wheat, vegetables, tobacco, and cotton; perennial grasses for grazing or forage; and woody crops like fruit trees and grapevines. Because the continuous annual land cover dataset is not available for the entire study area, we applied the

2005 land cover data for the period of 2000–2007 and the 2010 land cover data for the period of 2008–2016.

2.2.3. Crop classification maps

The crop classification maps were collected for validating the estimated crop phenology of different crop types. For the United States, we used the Cropland Data Layers (CDL), a high-resolution geo-referenced map made available by the U.S. Department of Agriculture (USDA). The CDL combines remotely sensed data with the ground truth survey and provides multi-year crop classification maps at a 30 m resolution for the conterminous United States (https://nassgeodata.gmu.edu/CropScape/). The historical CDL goes back as early as 1997 for North Dakota, and the national maps are available from 2008 to the present (https://www.nass.usda.gov/Research_and_Science/Cropland/metadata/meta.php). For Canada, we used the Agriculture and Agri-Food Canada (AAFC) data, which was developed using a range of high-resolution remotely sensed imagery (https://open.canada.ca/data/en/dataset). AAFC dataset provides the annual crop inventory product at 30 m resolution (56 m for the period of 2009–2010) across major agricultural regions in Canada during 2009–2017. The USDA CDL and AAFC crop distribution maps were used for extracting sites across the U.S. and Canada agrarian regions. For Mexico, there are no high-resolution crop classification time series maps available for the validation purpose. Instead, the Mexico crop map was derived from the International Food Policy Research Institute (IFPRI)'s Spatial Production Allocation Model (SPAM) Version 3.2, which represents a global fractional distribution of major crop types at a 5-arc-minute resolution for the period of 2004–2006 (You et al., 2014).

2.2.4. Climate data

Previous studies have indicated a strong relationship between the climate factors (e.g., average maximum/minimum daily air temperature) and crop phenology (He et al., 2015; Tao et al., 2006). In this study, we used daily spatially-interpolated air temperature from Daymet (Thornton et al., 2017) to examine the relationships between climate changes and crop phenological stages (planting dates and harvesting dates). The Daymet products provide estimates of daily weather parameters at 1 km resolution for North America during 1980–2017. These products have been widely used for biogeochemical modeling and climate change analysis at regional to continental scales (Liu et al., 2016a).

All the spatial datasets we collected were reprojected to the Albers equal-area projection and aggregated or downscaled to a 500 m resolution using the nearest neighbor algorithm in ArcGIS 10.3 to match the MODIS data.

2.3. Inventories of crop phenology

For the evaluation purpose, we collected ground data for the crop developmental stages from the crop progress reports for the U.S., crop reports for Canada, and statistics data for Mexico distributed by the USDA National Agricultural Statistics Service (NASS), Canada provincial ministries (Alberta, Manitoba, Ontario, and Saskatchewan), and USDA Foreign Agricultural Service (FAS), respectively. These data sets report typical crop growth dates categorized by crop types at the state-level in the U.S., provincial level in Canada, and country-level in Mexico, respectively. The USDA crop reports were updated weekly and averaged every five years and covered the period of 2005–2016, with phenological stages for each crop type clearly defined (https://www.nass.usda.gov/Publications/National_Crop_Progress/terms_definitions). These reports provided the percentages of major crops reaching a specific crop development stage (e.g., maize planted or soybean harvested) over the entire area of a particular state. They had the advantages of high reliability at the regional level. The dates of 80% progress of each recorded stage for corn, soybean, spring wheat, and cotton were extracted from the crop progress and condition graphs in USDA crop reports using the Web Plot Digitizer (https://automeris.io/WebPlotDigitizer). For Canada, the crop reports only include the planting dates and harvesting dates for four provinces, i.e., Alberta, Manitoba, Ontario, and Saskatchewan. Provincial crop reports provide tables showing crop progress ranging from 20% to 100% at various stages of barley, canola, soybean, spring wheat, and corn. All crop reports illustrated that the timing of each crop phenological stage varied greatly depending on crop types and regions. For Mexico, we used FAS statistics about crop planting and harvesting dates of corn and sorghum (https://ipad.fas.usda.gov/rssiws/al/crop_calendar/ca.aspx) for evaluating those derived from this study. Our collected data used for calibration and evaluation includes seven main crop types covering the period of 2005 – 2016.

For the U.S. and Canada, we used five-year averaged crop phenology records from the USDA/NASS to determine phenological thresholds and calibrate our improved approach. Accordingly, the weekly records were extracted from crop reports for evaluating our estimated crop phenological stages. For Mexico, the reported crop calendars in 2012 and 2017 were used for threshold settings and results evaluation, respectively.

Besides, the cropping intensity information in the U.S. was extracted from the USDA CDL datasets for validating the estimated crop rotation in this study. The satellite- and ground-based datasets used in this study were summarized in Table 1.

2.4. Methods

2.4.1. Deriving crop phenology descriptor

The MODIS data process software (MODIS Reprojection Tool, MRT) available from http://edcdaac.usgs.gov/datatools.asp was used to generate MOD09A1 products mosaics for North America for each 8-day composite image, respectively (Ren et al., 2008). MODIS products were re-projected from the sinusoidal projection to an Albers Equal-Area Conic projection, using the nearest neighbor resampling method, and to a 500 m resolution using MRT (Huete et al., 2002).

The EVI was calculated from the reflectances of the RED, BLUE, and NIR bands as follows (Huete et al., 1994).

$$EVI = 2.5 \times \frac{\rho_{NIR} - \rho_{RED}}{\rho_{NIR} + 6.0 \times \rho_{RED} - 7.5 \times \rho_{BLUE} + 1.0} \quad (1)$$

whereρ_{RED}, ρ_{NIR}, and ρ_{BLUE} are band 1 (0.620–0.670 μm), band 2 (0.841–0.876 μm), and band 3 (0.459–0.479 μm) reflectance from the MODIS products, respectively.

We first generated a cropland mask by aggregating the 250 m land cover dataset of North America (see Section 2.2.2) into 500 m and retained pixels with cropland percentages larger than 50%, which could reduce the influences of mixed pixels on crop phenology detection. All EVI processing and analyses were only conducted for cropland pixels for increasing computation efficiency. The EVI time series were smoothed with HANTS_IDL (Harmonic Analysis of NDVI Time Series). HANTS algorithm can smooth and reconstruct cloud-free remotely sensed vegetation datasets, such as NDVI, EVI, and Leaf Area Index (LAI) time series, and reduce the influence of clouds at the pixel level (Menenti et al., 1993; Zhang et al., 2015). Besides, it allows greater flexibility in the frequency choices and time series length than the Fast Fourier Transform (FFT) algorithm. HANTS is much more reliable than the straightforward FFT algorithm on removing the obvious outliers of the time series datasets (Zhou et al., 2015).

The smoothing process needs two input files, i.e., the original EVI time series and a cropland mask layer; only pixels with a value of 1 in the cropland mask layer were processed. Then the EVI time series in croplands were smoothed, and other land cover types were masked out (Roerink et al., 2000). Following these processes, the first and the second derivatives of the EVI curve were defined as follows.

$$f(x_i)' = \frac{f(x_i) - f(x_{i-1})}{8} \quad (2)$$

Table 1
Summary of the datasets used in this study.

Datasets	Spatial resolution	Timestep	Period	Data type	Data content	Purpose	Data source/description
MOD09A1	500 m	8-day	2000–2016	Raster	Reflectance	Building EVI time series	LP DAAC
Land cover (NA)	250 m	5-year	2005–2010	Raster	Cropland	Masking off non-cropland area	North American Land Change Monitoring System
Crop classification maps	30 m/56 m	Annual	2000–2016	Raster	Crop types	Providing individual map for evaluation of each crop type (U.S./Canada)	CDL of U.S./Agriculture Agri-Food Canada/Mexico
Meteorological data (NA)	1000 m	Daily	2000–2016	Raster	Climate factors	Providing temporal climatic factors	Daymet
Global fractional distribution of major crop types (SPAM)	5-min	–	2004–2006	Raster	Crop types	Providing individual map for evaluation of each crop type (Mexico)	IFPRI
Crop reports (the U.S. and Canada)	State/Province	5-year average	2005–2016	Document	Crop phenology	Using for setting thresholds	USDA NASS
Crop reports (the U.S. and Canada)	State/Province	Weekly	2005–2016	Document	Crop phenology	Evaluating estimation accuracy	USDA NASS
Crop calendar maps (Mexico)	Country	Average	–	Document	Crop phenology	Setting thresholds (2012) and evaluating estimation accuracy (2017)	FAS
Global Agro-ecological Zones (GAEZ v3.0)	5-min	–	2012	Vector	Ecological zones	Analyzing temporal trend of crop phenology in each ecological zone	GAEZ Module

$$f(x_i)'' = \frac{f(x_i)' - f(x_{i-1})'}{8} \quad (3)$$

where i is the sequence number of values in the time series (2, 3 … 46), the EVI curve has an

8-day time step, f and f' are smoothed and the first-order derivative of EVI time series, respectively. Accordingly, the first and second derivatives have 45 and 44 time series values from 2th to 46th image (DOY, Day of Year from 9 to 365) and 3th to 46th image (DOY from 17 to 365), respectively.

From Eqs. (2) and (3), the lengths of the first and second derivatives were shortened compared with the EVI time series. In this study, we did not make up the shortened periods because all phenological stages of seven major crop types were not observed during the shortened periods (DOY from 1 to 16) in North America (Appendix Table S1).

2.4.2. Cropping intensity and crop phenology extraction algorithms

In this study, the definitions of various crop phenological stages were from the USDA crop reports (https://www.nass.usda.gov/Publications/National_Crop_Progress/terms_definitions, Table 2). It has been widely accepted that EVI values could reflect the plant canopy development (Huete et al., 1999; Jiang et al., 2008). The transition dates of VI time series curves could characterize the seasonal dynamics of some crop growth stages, which have been used for identifying typical crop phenological stages (Xin et al., 2002; Liu et al., 2017a,b). Specifically, EVI can reduce sensitivity to the soil, non-photosynthetically active vegetation, and atmospheric effects, but remains sensitive to changes in canopy structure and density in cases where NDVI loses sensitivity (Zhang et al., 2019).

In this study, we improved the EVI-curve-based approach through (1) using transition dates of the EVI time series, first/second derivatives of the EVI time series to identify crop phenological stages; (2) setting flexible thresholds for five crop phenological stages according to the ground survey data; (3) expanding to detect five main crop phenological stages for seven crop types.

– Extracting cropland and cropping intensity

Previous studies have verified that maximum NDVI occurs around the heading dates (Sakamoto et al., 2005; Xin et al., 2002). In this study, we took the EVI peaks as the heading date for each crop type (See the details in the section of Extracting five crop phenological stages). We set a maximum EVI threshold of 0.35 (Li et al., 2014; Liu et al., 2016a; Zhang et al., 2015) to exclude the non-croplands areas, i.e., the pixels with the maximum EVI values less than 0.35 were not included in the computation. Furthermore, we analyzed the ground data from crop reports and found that the intervals of two crop-heading dates in the double-cropping system were more than 80 days across North America. This interval represents a useful parameter for determining a multi-cropping system (Sakamoto et al., 2006). Therefore, we set a threshold of 80-day for further identifying the double cropping system, i.e., if the interval between two EVI peaks is larger than 80 days, the pixel will be identified as the double cropping system.

In addition, we also set a threshold for confining the time range of crop heading dates. The ground-based crop phenological information suggested that the heading dates of most crops occurred between the DOY (Day of Year) 150 and 260 in the U.S. (Appendix Table S1). Also, Sakamoto (2018) analyzed the EVI time series and detected the crop planting dates and harvesting dates as 60 days before the estimated heading dates and 30 days after the heading dates, respectively. Therefore, we set a more flexible time range (DOY, 73–297) as the threshold of heading dates for the entire North America. The peaks of the EVI curve falling outside this range were excluded. The criteria mentioned above can be described by the following conditions to identify cropping intensity:

Table 2
Phenology definition of different crop types.

Phenological stages	Crop types						
	Barley	Canola	Corn	Cotton	Soybean	Spring wheat	Sorghum
Planting	Planting	Planting	Planting	Planting	Planting	Planting	Planting
Jointing	–	–	–	Squaring	–	Jointing	–
Heading	Headed	–	Silking	Setting Bolls	Blooming	Headed	Headed
Maturity	–	–	Mature	–	Dropping leave	Mature	Mature
Harvesting	Harvesting	Harvesting	Harvesting	Harvesting	Harvesting	Harvesting	Harvesting

$$\begin{cases} \begin{cases} f(x_i)' > 0 \\ f(x_{i+1})' < 0 \\ f(x_{i+1}) \geq 0.35 \end{cases} \\ 73 < T < 297 \\ \Delta T = Ti - Tj > 80, \quad When \ n \geq 2 \end{cases} \tag{4}$$

WHERE f' is the first-order derivative of EVI curve; f is smoothed EVI curve; i/jmeans the *ith/jth* of EVI/EVI' values in the time series (1, 2, 3… 46), T is the DOY of EVI peak, ΔT is the time interval of two peaks of the EVI curve. We, therefore, obtained cropping intensity n (Single-cropping system: $n = 1$ and double-cropping system: $n = 2$).

– Extracting five crop phenological stages

Heading dates

The heading dates are reached when transforming from the vegetative stage to the reproductive stage, after which leaves begin to turn yellow and wither (Sakamoto et al., 2005). In this study, we identified the heading date ($T_{heading1}$ for the single-cropping system and $T_{heading1}$, and $T_{heading2}$ for the double-cropping system) as the date that the maximum MODIS EVI occurs in the time profiles (Xin et al., 2002; Xu et al., 2017; Yan et al., 2019). Based on the summarized ground data from crop reports (see Section 2.3), we found that the crop growing season is typically less than 220 days for major crop types (Appendix Table S1). We thereby confined the crop growing season within the range of 110 days before and after the estimated heading date (Fig. 1; Appendix Fig. S1; Table 3). The identification of the temporal thresholds for constraining predicted values can reduce the interferences caused by data noise.

Planting dates

In general, agricultural lands are plowed or cultivated before crop planting. At the planting dates, photosynthetic activity does not start, and crop leaves begin to grow after the planting dates. The EVI curve shows lower values during this period and then starts increasing after crop planting. It is reasonable to assume that the planting date is located at the lowest point of the EVI profile during the early growth stage. This lowest point corresponds to the peak of the second-order derivative of the EVI curve (before the heading date), after which the EVI value begins to increase (Fig. 1B and D). We then identified the crop planting dates by detecting when the second-order derivative of the EVI curve reaches the first peak before the heading dates. Based on the ground data, the planting dates were constrained to occur within the time range of

Table 3
Transition dates and thresholds from time series curves for identifying phenological stages.

Phenological stages	Descriptions	Range with thresholds (Day of Year, DOY)
Heading: $T_{heading1}$	The first peak of EVI time series	
Planting: $T_{planting1}$	The peak of the 2nd derivative	[$T_{heading1}$ − 110, $T_{heading1}$ − 40]
Jointing: $T_{jointing1}$	The peak of the 1st derivative	[$T_{heading1}$ − 90, $T_{heading1}$ − 20]
Maturity: $T_{maturity1}$	The trough of the 1st derivative	[$T_{heading1}$ + 20, $T_{heading1}$ + 90]
Harvesting: $T_{harvesting1}$	The peak of the 2nd derivative	[$T_{heading1}$ + 30, $T_{heading1}$ + 110]
Heading: $T_{heading2}$	The second peak of EVI time series	
Planting: $T_{planting2}$	The peak of the 2nd derivative	[$T_{heading2}$ −110, $T_{heading2}$ − 40]
Jointing: $T_{jointing2}$	The peak of the 1st derivative	[$T_{heading2}$ − 90, $T_{heading2}$ − 20]
Maturity: $T_{maturity2}$	The trough of the 1st derivative	[$T_{heading2}$ + 20, $T_{heading2}$ + 90]
Harvesting: $T_{harvesting2}$	The peak of 2nd derivative	[$T_{heading2}$ + 30, $T_{heading2}$ + 110]

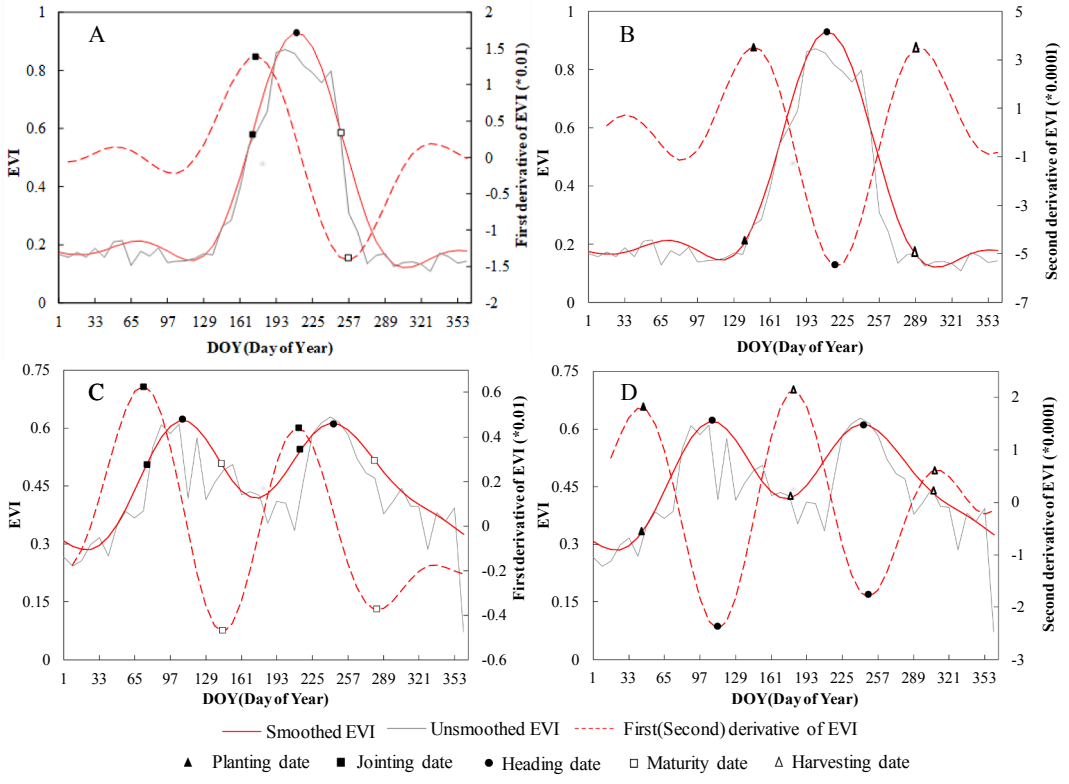

Fig. 1. Crop phenological stages extracted using the first and second derivatives of the EVI curve for the single-cropping system (A, B) and double-cropping system (C, D).

40–110 days before the estimated heading dates (Table 3).

Jointing dates

The jointing dates occur after the planting dates and before the heading dates. At this stage, the crop canopy expands rapidly to meet the active photosynthetic activity. Accordingly, EVI value increases with a higher rate than other stages (Fig. 1A and 1C). In this study, we identified the jointing date by detecting the peak of the first-order derivative of the EVI curve (before the heading date), i.e., the fastest growing point of EVI values. To reduce the impact of outliers, we set a threshold of 20–90 days before the heading dates by referring to the crop reports.

Maturity dates

The maturity dates take place during the period plant leaf begins to lose activity or change color after the heading dates and before the harvesting dates. During this period, photosynthetic activity and green leaf area decrease rapidly. The trough of the first-order derivative of the EVI curve (after the heading date) represents the fastest declining point of EVI values. We then defined the point in the EVI time series curve with a maximum reduction rate as the crop maturity dates (Fig. 1A and C). Similar to other phenological stages, we also set an appropriate threshold with a range of 20–90 days after the heading dates for the maturity dates (Table 3).

Harvesting dates

In the harvesting season, leaves of crop plants continue to wither and die after the maturity stage. Crop canopies are generally harvested in this stage. Correspondingly, EVI values continue to decrease and go to the lowest point when the crop harvested from fields. The peak of the second-order derivative of the EVI curve after the heading date corresponds to the lowest value of EVI during the crop growth period (Fig. 1B and D). Here we used this key point to detect the harvesting date. Similarly, based on the ground data, the harvesting dates were constrained to occur within the time range of 30–110 days after the estimated heading dates.

All thresholds we used for identified five phenological stages (Table 3) were based on the ground information recorded in crop reports (Appendix Table S1). These thresholds represent the relative time ranges, which depend on the dynamic pattern of the EVI curves.

Wheat-soybean is the most popular double cropping system in the study area (Kelley and Sweeney, 2005; Borchers et al., 2014; Marra and Carlson, 1986). Winter varieties were usually planted each fall directly following soybean harvest in early October (Heggenstaller et al., 2008). USDA report (Marra and Carlson, 1986) suggested that the winter wheat is generally harvested in the morning and soybeans planted in the afternoon of the same day in the same field, especially when conservation tillage is applied. In some cases, the growing season for the second cropping system could be shortened because of the overlap in harvesting the first crop and planting the second (Marra and Carlson, 1986). Therefore, in this study, we detected the harvesting date of the first season as the planting date of the second season.

Fig. 2 shows a study flowchart summarizing the systematic processes of identifying crop phenological stages.

2.5. Accuracy evaluation

2.5.1. Evaluation of the satellite-based cropping intensity

For evaluating the cropping intensity results, we randomly chose a total of 1006 sites, including the single-cropping system and the double-cropping system distributed across twelve regions in the United States based on the 2016 CDL data (Appendix Table S2). Each site consists of a polygon delineated on CDL maps via manual interpretation, ensuring that the verification datasets are widely distributed geographically. The size of the evaluation sites ranged from 1 pixel (~0.25 km^2) to 79 pixels (~19.75 km^2), and these sites covered 6000 MODIS pixels.

The confusion matrix was applied to evaluate the estimated cropping intensity. It includes the overall accuracy (OA), Kappa coefficient (Kappa), producer's accuracy (PA), and user's accuracy (UA) (Fitzgerald and Lees, 1994; Næsset, 1996). The overall accuracy represents the percentage of estimated samples that are correctly identified (Hubert-Moy et al., 2001). The Kappa coefficient measures the agreement between observations and prediction results. Kappa coefficient value of 1 represents a perfect agreement, while a value of 0 means no agreement. The producer's accuracy is a measure of the omission error, defined as the number of correctly classified pixels relative to the total number of pixels used in the assessment for a specific class. The user's accuracy is a measure of the commission error associated with a class, which is derived from the number of pixels correctly allocated to a class relative to the total number of pixels predicted to belong to that class (Foody, et al., 2006). Overall accuracy and the Kappa coefficient were computed as follows (Congalton, 1991):

$$Overall\ Accuracy = \frac{Total\ number\ of\ correct\ estimaitons}{Total\ number\ of\ dataset} \quad (5)$$

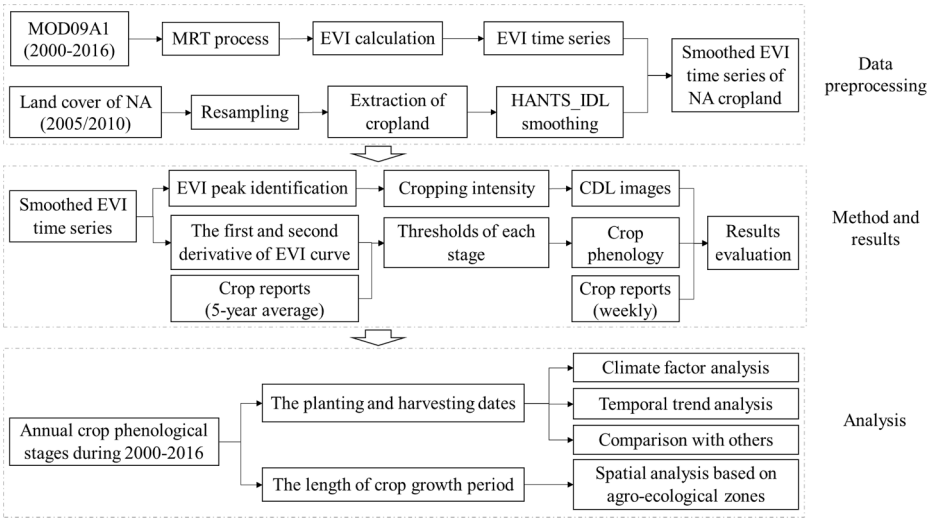

Fig. 2. Study flow chart.

$$\text{Kappa} = \frac{N\sum_{i=1}^{r} x_{ii} - \sum_{i=1}^{r}(x_{i+} \times x_{+i})}{N^2 - \sum_{i=1}^{r}(x_{i+} \times x_{+i})} \quad (6)$$

where r is the number of rows in the matrix, $x_{ii}$is the number of observations in rowiand columni, x_{i+} and x_{+i} are the marginal totals of row i and column i, respectively, and N is the total number of observations.

2.5.2. Evaluation of the satellite-based crop phenology

We evaluated our estimated crop phenology results against ground information recorded in crop progress reports from USDA, NASS, Canada provinces, and FAS (Table 4). Crop classification maps included CDL for the U.S., AAFC for Canada, and crop map derived from SPAM for Mexico. We summarized crop phenology of six main crop types (corn, soybean, spring wheat, barley, sorghum, and cotton) for the U.S. from USDA NASS crop progress reports, five major crop types (barley, canola, soybean, spring wheat, and corn) for Canada from the crop reports of five provinces, and two crop types (corn and sorghum) for Mexico from the FAS reports (Table 4). These seven crop types comprise more than 65% of the total crop area in North America (USDA NASS Census of Agriculture in 2017). For each crop type, we selected major producing states or provinces to evaluate estimated phenological stages (Table 4). In these states or provinces, we chose pixels that the targeted crop types accounted for more than 80% to compare against satellite-derived crop phenology. Limited by the data availability, we separately evaluated corn and soybean by randomly selecting 75 sites to assess the accuracy of satellite-based crop phenology in Mexico from 2004 to 2016. Pixels in the center of larger patches were selected to reduce the influence of mixed pixels during this process.

Table 4
Data used for estimated phenological stages evaluation.

ID	Crop types	Years	Phenological stages	Countries	States/Provinces
1	Corn	2004–2016	Planting Heading Maturity Harvesting	The U.S. Canada Mexico	Colorado; Ohio; Illinois; Indiana; Iowa; Kansas; Kentucky; Michigan; Minnesota; Missouri; Nebraska; North Dakota; South Dakota; Ontario
2	Soybean	2005–2016	Planting Heading Maturity Harvesting	The U.S. Canada	Arkansas; Illinois; Indiana; Iowa; Kansas; Kentucky; Louisiana; Michigan; Minnesota; Mississippi; Ontario; Manitoba
3	Cotton	2006–2016	Planting Jointing Heading Harvesting	The U.S.	Alabama; Arizona; Arkansas; California; Georgia
4	Spring wheat	2005–2016	Planting Jointing Heading Maturity Harvesting	The U.S. Canada	Idaho; Minnesota; Montana; North Dakota; South Dakota; Alberta; Saskatchewan; Manitoba
5	Barley	2009–2016	Planting Heading Harvesting	The U.S. Canada	Colorado; Montana; Oregon; Utah; Washington; Wyoming; Alberta; Saskatchewan; Manitoba
6	Canola	2009–2016	Planting Harvesting	Canada	Alberta; Manitoba; Saskatchewan; Ontario
7	Sorghum	2004–2006	Planting Heading Maturity Harvesting	The U.S. Mexico	Colorado; Kansas; Oklahoma; South Dakota; Texas

We used the coefficient of determination (R^2), root mean square error (*RMSE*), and mean absolute error (*MAE*) to evaluate the estimated crop phenological stages. In general, a higher R^2, a lower RMSE, and a lower MAE mean higher accuracies of the estimation:

$$R^2 = \frac{\sum_{i=1}^{n}(x_i - \bar{x})^2(y_i - \bar{y})^2}{\sum_{i=1}^{n}(x_i - \bar{x})^2\sum_{i=1}^{n}(y_i - \bar{y})^2} \quad (7)$$

$$RMSE = \sqrt{\frac{1}{n}\sum_{i=1}^{n}(y_i - x_i)^2} \quad (8)$$

$$MAE = \frac{1}{n}\sum_{i=1}^{n}|y_i - x_i| \quad (9)$$

where n represents the number of comparisons; y_i and x_i are estimated phenological dates in this study and those derived from ground information, respectively.

2.6. Mann–Kendall test and Sen's slope estimator

In this study, we used the Mann–Kendall test (Gilbert, 1987; Chmielewski et al., 2004; Li et al., 2014) and the Sen's slope estimator (Sen, 1968) to identify statistically significant monotonic trends in estimated planting dates, harvesting dates, and length of the crop growing season. We analyzed the temporal trends of crop planting and harvesting dates (the single cropping system and the first season of the double cropping system) using the Mann-Kendall test and the Sen's slope. Further, we also tested the interannual variation of cropping systems in North America during the study period. The statistical analysis was implemented using the R computing environment (R Development Core Team, 2011).

We followed Sen (1968) to calculate the slope or the time series as:

$$Q_{j,k} = \frac{x_j - x_k}{j - k} \quad (10)$$

where $k < j$, $k = 1, 2, \ldots, n-11$, and $j = k + 1, k + 2, \ldots, n$; x_j and x_k are the crop phenological stage for year j and k, respectively; n is the length of the time series.

Therefore, a total of $n(n-1)/2$ elements of $Q_{j,k}$ and their median is the slope, or trend, of the temporal phenological stages series.

The significance of the slope was tested using the Mann–Kendall statistic (Gilbert, 1987), in which we first calculated the parameter S as:

$$S = \sum_{k=1}^{n-1}\sum_{j=k+1}^{n} sign(x_j - x_k) \quad (11)$$

where $sign(x_j - x_k)$ is -1, 0, or $+1$ if $(x_j - x_k)$ is <0, $=0$, or >0, respectively. Then we calculated parameter V as:

$$V = \frac{1}{18}[n(n-1)(2n-5) - \sum_{p=1}^{g} t_p(t_p - 1)(2t_p + 5)] \quad (12)$$

where g is the number of tied groups. A tied group is a set of sample data that have the same value and t_p is the number of years in the p_{th} tied group. If there are no tied groups, this summation process can be ignored (Kisi and Ay, 2014). At last, the test statistic Z was calculated as:

$$Z = \begin{cases} \frac{S-1}{\sqrt{V}}, & if \ S > 0 \\ 0, & if \ S = 0 \\ \frac{S+1}{\sqrt{V}}, & if \ S < 0 \end{cases} \quad (13)$$

Positive values of Z indicate increasing trends, while negative Z values show decreasing trends. Testing trends was performed at the specific α significance level. If $Z > Z_{0.90} = 1.65$, $Z > Z_{0.95} = 1.96$, or $Z > Z_{0.99} = 2.58$, the slope estimated by $Q_{j,k}$ is significant at 90%, 95%, and 99% confidence level, respectively.

2.7. Climate datasets

To examine climate change impacts, we correlated our estimated crop phenology to daily air temperatures over North America during 2000–2016. Average daily minimum/maximum temperatures during crop planting season (April to June) and harvesting season (August to October) were calculated based on the Daymet climate datasets (Thornton et al., 2017).

3. Results

3.1. Evaluation of the satellite-based cropping intensity

Based on the CDL datasets, we mapped the spatial distribution of the single- and double- cropping systems using the feature extraction tool in ArcGIS 10.3. Accuracies of the estimated cropping intensity were evaluated against the CDL-based maps for twelve USDA-defined sub-regions in the U.S. for the year 2016 (Table 5). Our results showed that user's accuracies were higher than 60% in ten regions, which varied from 60% to 93.67%. The producer's accuracies in seven regions reached 60% except for the double-cropping system in Mountain, Pacific, and Southern Plains. Seven regions had overall accuracies over 80%. Particularly, accuracies in three major agricultural regions (Heartland, Upper Midwest, and Great Lakes) were higher than 85%. Relatively low accuracies (<75%) were found in the Mountain, Northwest, and Pacific regions where agricultural areas are generally more fragmented. For kappa coefficients, values ranged from 0.29 to 0.73, with 7/10 regions being over 0.55.

3.2. Evaluation of the satellite-derived crop phenology

Based on our estimated phenological stages, we calculated the dates of 80% (the U.S.) and 20–100% (Canada) progress of crops and compared them against those from the crop reports (Table 6 in the U.S. and Table 7 in Canada). Generally, the R^2 values were higher than 0.60, the RMSEs were lower than ten days, and the MAEs were lower than eight days for all predicted phenological stages, except for soybean in Canada ($R^2 = 0.35$). Our results demonstrated a relatively high accuracy for predicting the major crop phenological stages. In the U.S., evaluation results showed that more than half of the values of R^2 (13/24) were higher than 0.80. For sorghum in the U.S., all R^2 values were higher than 0.90, RMSEs were lower than five days, and MAEs were lower than four days. For Canada, only three of ten R^2 values were lower than 0.70, all RMSEs were lower than eight days, and MAEs were lower than seven days. Relatively higher accuracies were found for corn ($R^2 = 0.99$) and soybean ($R^2 = 0.90$) harvesting dates in Canada compared to those in the U.S. The relatively larger errors for soybean (planting dates) in Canada might be attributed to the small sample sizes and different ground data acquisition methods.

Previous studies have reported differences between the remote sensing-based crop planting estimations and those reported by ground observations. For example, Hmimina et al. (2013) found the differences were 10.5 and 24.2 days between the crop phenological dates derived from the MODIS daily and 16-day products, respectively. Ortiz-Monasterio and Lobell (2007) reported that approximately one-week difference was found between the observed and estimated crop planting dates. In this study, our results showed that the differences were lower than seven days between the estimated planting dates and crop reports for all crop types, except the corn in the U.S. (7.62 days). It illustrated that the key points used for detecting crop planting dates could capture the event well.

For each phenological stage of seven major crops, we plotted the time ranges of the satellite-based crop phenological dates and ground recorded data (Appendix Fig. S2 A–E: The U.S., F, and G: Canada, H and I: Mexico). For the U.S., some crop phenological stages were not included in the comparisons because no records are available in the crop reports. Similarly, for Canada and Mexico, we only analyzed planting and harvesting dates due to limited data availability. Our evaluation results suggested that the satellite-based major crop phenological dates closely matched those from the ground observation in the U.S. and Canada (Appendix Fig. S2 A–G). For Mexico, the validation of planting dates and harvesting dates for corn and sorghum also exhibited a high agreement with FAS recorded datasets. Over 80% of the predicted phenological dates were within the recorded range of crop calendar datasets from FAS, except for the harvesting dates of corn (Appendix Fig. S2 H and I).

3.3. Comparison with existing datasets and studies

We evaluated our results against crop planting and harvesting dates from two previous studies. The Crop Calendar Dataset provides *in situ* observations of crop planting and harvesting dates derived from FAO and USDA census in 2007 and 2008 (Sacks et al., 2010). The SACRA (the SAtellite-derived CRop calendar for Agricultural simulations) dataset represents the estimated global sowing and harvesting dates based on the time series of averaged VEGETATION/SPOT NDVI during 2004–2006 (Kotsuki and Tanaka, 2015).

Our comparisons (Tables 8 and 9) suggested that our estimated

Table 5
Accuracies (%) of satellite-estimated cropping intensity in the U.S. for the year 2016.

Regions		Heartland	Mountain	Northern Plain	Northwest**	Pacific	Upper Midwest**
Single crop	PA*	96.83	82.63	77.35	-	87.10	–
	UA*	89.25	68.32	77.81	-	74.81	–
Double crop	PA	67.59	44.69	77.27	–	39.76	–
	UA	88.48	64.05	76.81	–	60.00	–
OA*		89.09	67.11	77.31	71.97	71.60	88.05
Kappa		0.70	0.29	0.55	–	0.29	–
Regions		**Delta**	**Eastern Mountain**	**Great Lakes**	**Northeastern**	**Southern**	**Southern Plains**
Single crop	PA	85.36	88.59	89.50	61.05	89.74	91.69
	UA	93.35	78.98	87.30	77.21	70.85	74.95
Double crop	PA	81.95	83.64	82.78	90.72	80.43	50.63
	UA	65.37	91.35	85.63	81.89	93.67	79.09
OA		84.50	85.67	86.60	80.63	83.66	75.96
Kappa		0.62	0.71	0.73	0.55	0.66	0.45

* PA, UA, and OA represent the producer's accuracy, user's accuracy, and overall accuracy, respectively.
** These two regions only have single cropping systems.

Table 6
Evaluation of the satellite-estimated phenological stages in the U.S.

Stages	Statistics	Corn	Soybean	Spring wheat	Cotton	Barley	Sorghum
Planting	RMSE (days)	9.13	6.84	5.63	9.71	4.11	4.54
	MAE (days)	7.62	5.56	4.12	6.10	2.71	3.62
	R^2	0.65**	0.76**	0.87**	0.81**	0.85**	0.94**
	N	98	84	43	42	34	45
Jointing	RMSE (days)	–	–	5.6	6.19	–	–
	MAE (days)	–	–	5.33	4.58	–	–
	R^2	–	–	0.96**	0.60**	–	–
	N	–	–	6	43	–	–
Heading	RMSE (days)	5.42	8.50	5.58	8.29	3.03	4.95
	MAE (days)	4.42	7.41	4.42	6.26	2.32	3.73
	R^2	0.77**	0.65**	0.80**	0.63**	0.93**	0.96**
	N	110	79	45	43	34	45
Maturity	RMSE (days)	6.26	4.70	6.10	–	–	5.03
	MAE (days)	5.18	3.98	4.75	–	–	3.56
	R^2	0.81**	0.71**	0.63	–	–	0.97**
	N	111	83	4	–	–	45
Harvesting	RMSE (days)	6.48	8.11	7.56	3.75	9.52	4.42
	MAE (days)	4.91	6.50	6.37	3.04	8.26	3.42
	R^2	0.77**	0.66**	0.80**	0.88**	0.79**	0.96**
	N	110	83	38	45	27	45

Note. N represents the number of states or provinces used for evaluation.
** Represents a 1% significance level.

Table 7
Evaluation of the satellite-estimated phenological stages in Canada.

Stages	Statistics	Corn	Soybean	Spring wheat	Barley	Canola
Planting	RMSE (days)	6.94	7.71	4.68	5.58	6.03
	MAE (days)	6.20	6.70	3.75	4.56	5.18
	R^2	0.72*	0.35*	0.77**	0.77**	0.63**
	N	10	10	12	18	22
Harvesting	RMSE (days)	4.42	6.36	3.45	7.88	6.22
	MAE (days)	3.50	4.50	3.00	6.5	5.15
	R^2	0.99*	0.90*	0.75**	0.62**	0.84**
	N	4	6	11	16	20

Note. N represents the number of states or provinces used for evaluation.
* Represents a 5% significance level.
** Represents a 1% significance level.

planting dates were slightly later than the Crop Calendar Dataset in 19 of the total 23 states considered in the comparison, while the harvesting dates were relatively earlier in 12 states. In most states, discrepancies between our estimated planting dates or harvesting dates and those from the Crop Calendar Dataset were less than 15 days (Table 8). Crop Calendar Dataset was digitized from ground observations derived from several different resources, most of which were specified for an entire country or a sizeable sub-national unit (e.g., a single state in the US). Lacking valuable spatial information of crop phenology could limit the application of the dataset at the regional or landscape scales. Moreover, the dataset does not capture any phenological changes in time, which only refers to planting and harvesting dates for the 1990s or early 2000s. The comparison between our estimates with the SACRA suggested large discrepancies in both planting dates/harvesting dates; in particular, three crop types except for spring wheat displayed large differences in planting dates in North Dakota (Table 9). This could be partly attributed to the fact that the SACRA dataset only selected one dominant crop in each administrative unit. Moreover, it was produced using the time series of the NDVI averaged from three consecutive years (2004–2006) at a resolution of 5 arcmin. We further compared our estimated planting and harvest dates with those from the SACRA at the state level using the USDA crop reports for the period 2004–2006 (Appendix Table S3). The results showed that our estimates (RMSEs and MAEs lower than 15 days) had a better performance than the SACRA (RMSEs and MAEs were larger than 22 and 12 days, respectively).

Besides, to verify the robustness of our improved approach, we also compared our results with the phenological stages derived from the same key points but without setting thresholds. Higher accuracies were found for the estimations of all crop types detected from the improved EVI-curve-based approach (Appendix Table S4).

3.4. Spatial and temporal patterns in cropping intensity

The satellite-based cropping intensity maps showed evident spatial patterns in North America (Fig. 3). The agriculture in North America was dominated by the single-cropping system during the study period, which mainly occurred in Canada and the northern U.S. The double cropping system was primarily distributed in Mexico, the southern U.S., and parts of the southeastern U.S. Single-cropping system dominated in Canada and was relatively stable during 2000–2016. There were no noticeable spatial transitions of cropping intensity in Mexico during the study period.

Only two years of the results are presented, but the general patterns of cropping intensity remained roughly constant throughout the study period, although an expansion of double-cropping areas was found in the lower Great Plains.

Table 10 showed the results of the Mann-Kendall test and Sen's slope of cropping intensity in North America. A significant increasing trend was detected in the single cropping system with a rate of 5,489,000 acres per year at the 1% significance level. However, no significant trend was found for the double-cropping system.

3.5. Spatial and temporal patterns in crop planting and harvesting dates

The spatial patterns of planting and harvesting dates in the single-cropping system and the first season of the double-cropping system for the year 2016 were shown in Fig. 4. Spatially, the crop planting dates in the northern areas of North America (e.g., Canadian Prairies, the north of the US Midwest and Great Plain) were generally later than those in most of the southern regions. The planting dates showed a slightly increasing trend with latitudinal gradients between 20°N and 70°N

Table 8
Comparison of the estimated planting and harvesting dates versus Sacks et al. (2010) at the state level.

States	Crop types	Planting date (DOY)		Difference (days)	Harvesting date (DOY)		Difference (days)
		Results (2007–2008)	Sacks et al. (2010)	Results (2007–2008) – Sacks et al.(2010)	Results (2007–2008)	Sacks et al. (2010)	Results(2007–2008) – Sacks et al.(2010)
IL	Corn	151	130	21	295	295	0
MN	Corn	149	136	13	296	302	−6
NE	Corn	149	131	18	291	299	−8
MI	Corn	136	136	0	285	306	−21
CO	Corn	145	128	17	287	304	−17
AR	Corn	123	119	4	263	256	7
IN	Corn	148	138	10	292	303	−11
KS	Corn	130	122	8	274	281	−7
MO	Corn	139	128	11	282	289	−7
ND	Corn	146	139	7	291	292	−1
OH	Corn	146	137	9	293	298	−5
SD	Corn	145	141	4	290	300	−10
NC	Corn	111	115	−4	241	271	**−30**
TX	Corn	93	97	−4	232	251	−19
IA	Soybean	165	146	19	304	282	22
MI	Soybean	169	147	22	305	292	13
IL	Soybean	149	147	2	297	286	11
IN	Soybean	161	148	13	297	289	8
OH	Soybean	165	150	15	305	289	16
MN	Soybean	165	150	15	301	286	15
WI	Soybean	157	153	4	301	294	7
NE	Soybean	161	158	3	305	291	14
MO	Soybean	169	158	11	309	298	11
MAE (days)				10.17			11.57
RMSE (days)				12.00			13.46

Note. The comparison focused on 2007–2008, consistent with the study period in Sacks et al. (2010).

Table 9
Comparison of the estimated planting and harvesting dates versus SACRA at the state level.

States	Crop types	Planting date (DOY)		Difference (days)	Harvesting date (DOY)		Difference (days)
		Results (2004–2006)	SACRA	Results (2004–2006) –SACRA	Results (2004–2006)	SACRA	Results (2004–2006) – SACRA
IL	Corn	140	82	58	284	249	35
MN	Corn	149	98	51	296	259	37
NE	Corn	146	95	51	291	243	48
MI	Corn	136	108	28	285	264	21
AR	Soybean	139	80	59	280	264	16
IN	Soybean	146	99	47	287	262	25
MO	Soybean	136	92	44	283	253	30
OH	Soybean	148	118	30	290	257	33
SD	Soybean	146	110	36	292	263	29
NC	Soybean	131	91	40	277	299	−22
SC	Soybean	125	93	32	273	307	−34
MS	Soybean	126	87	39	271	299	−28
LA	Soybean	123	83	40	265	293	−28
ND	Spring wheat	127	144	17	267	234	33
GA	Cotton	138	79	59	299	329	30
MAE (days)				42.07			29.93
RMSE (days)				39.92			28.13

Note. The comparison focused on 2004–2006, consistent with the study period in Kotsuki and Tanaka (2015).

latitude (Fig. 4A). The estimated results for crop harvesting dates showed a similar spatial trend to that of the planting dates, which later harvesting dates occurred in the Canadian Prairies, much of the US Midwest and parts of the northern Great Plain (Fig. 4B). This phenological trend in planting and harvesting dates characterized the spatial variability in geographic patterns and might be explained by climatic temperature and distributions of different crop types. In most croplands of Mexico, the crop planting dates generally began from 140 to 180 (Julian Day), and harvesting dates mainly fell into the range of 280–320 (Julian Day).

We further performed a temporal trend analysis for crop planting/harvesting dates (Fig. 5) and summarized in Fig. 6. Sen's slope represents the changing trends during the study period in Fig. 5. For the planting dates, approximately half of the evaluated pixels showed negative trends, less than a quarter showed positive trends, and the rest of the areas showed no significant trends. The pixels with advanced planting dates were sparsely distributed across North America. For harvesting dates, the areas with delayed trends were mainly clustered in the mid and high latitudes of North America. In particular, croplands in Canadian Prairies and the north of the Mississippi River in the U.S. showed delayed harvesting dates. However, only approximately 10% ($p < 0.1$) of the evaluated areas over North America witnessed significant changes in both planting and harvesting dates during the period 2000–2016.

To investigate the crop phenology trends at the continental scale, we first separately computed the spatial averages of planting and harvesting

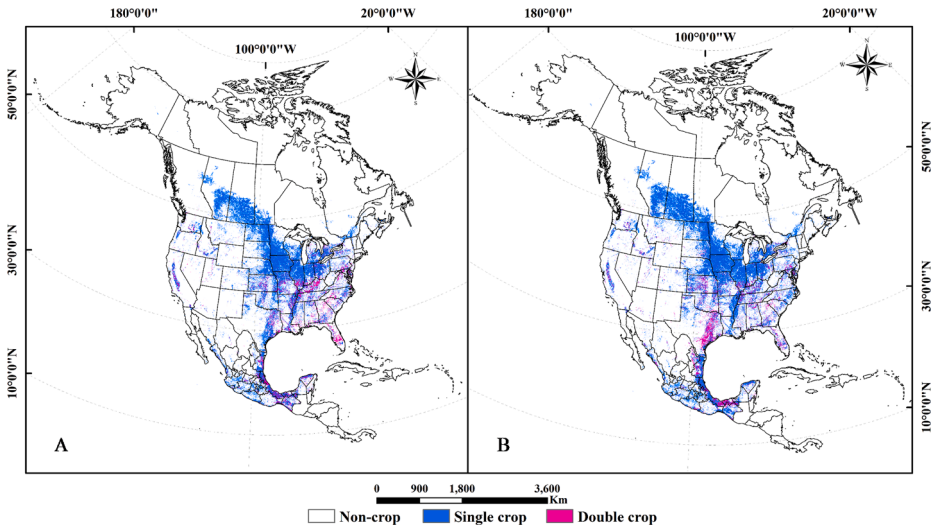

Fig. 3. Distribution of the single and double-cropping systems across North America in 2000 (A) and 2016 (B).

Table 10
Temporal trends of cropping intensity using Mann-Kendall test and Sen's slope.

Crop rotation	Test	
	Mann-Kendall test (Z)	Sen's slope (*1000 acres)
Single crop	2.68	5489*
Double crop	−0.29	−1432

* Represents a 1% significance level.

dates and then fitted their changing patterns during the study period (Fig. 6). For the areas with significant changes, we found that the planting dates of the first growing season advanced by 0.60 days/year ($p < 0.01$), or about 10.20 days over the entire study period. For the harvesting dates in areas with significant trends, our results suggested a delaying trend at a rate of 0.78 days/year ($p < 0.01$), i.e., 13.26 days over the entire study period. We further divided entire North America into 14 sub-regions, including Canada, Mexico, and twelve regions of the U.S. (Appendix Table S2). Of the 14 sub-regions, 11 experienced an advancement in the planting dates during the study period, which accounted for 72.5% of the total areas with statistically significant changes; 9 sub-regions postponed in harvesting dates, accounting for 75.5% of the total areas with statistically significant changes (Appendix Fig. S4). Regionally, the northern and eastern parts of North America were found to have experienced the most significant delays in crop harvesting dates.

3.6. Climate change impacts on crop phenology

3.6.1. Temporal trend analysis of crop growing season length based on thermal zones

Fig. 7 displays the spatial distribution of the changing trends of crop growing season length as calculated from the planting and harvesting dates during the study period. Positive values (blue) and negative values (red) represent the prolonged growing season and shortened growing seasons, respectively. During the study period, the averaged crop growing seasons have extended at a rate of 0.33 days/year ($P < 0.01$) over North America. The extension of crop growing seasons is mainly concentrated in the U.S. and Canada (>30°N) with higher significance (Fig. 7). In contrast, most areas of Mexico (<30°N) indicated shortened crop growing seasons. In addition, areas with extended growing seasons (slope > 0) displayed a gradual increase along with increasing latitude in North America (Fig. 7A).

Based on the Global Agro-ecological Zones (GAEZ v3.0, http://www.fao.org/nr/gaez/en/) (Appendix Fig. S5), we further performed a trend analysis to characterize the temporal variations in the length of the crop growing season. North America is classified into 12 zones in the GAEZ

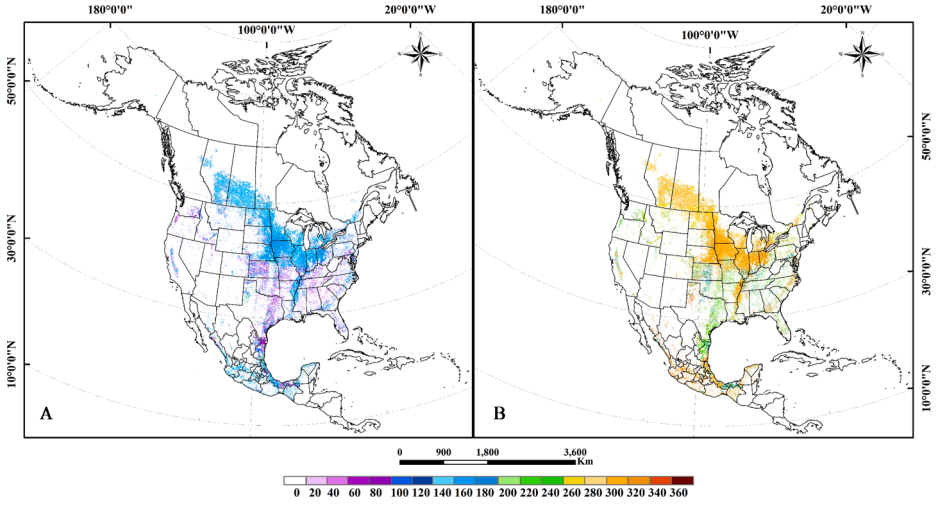

Fig. 4. Estimated planting dates (A) and harvesting dates (B) of the first growing season across North America in 2016.

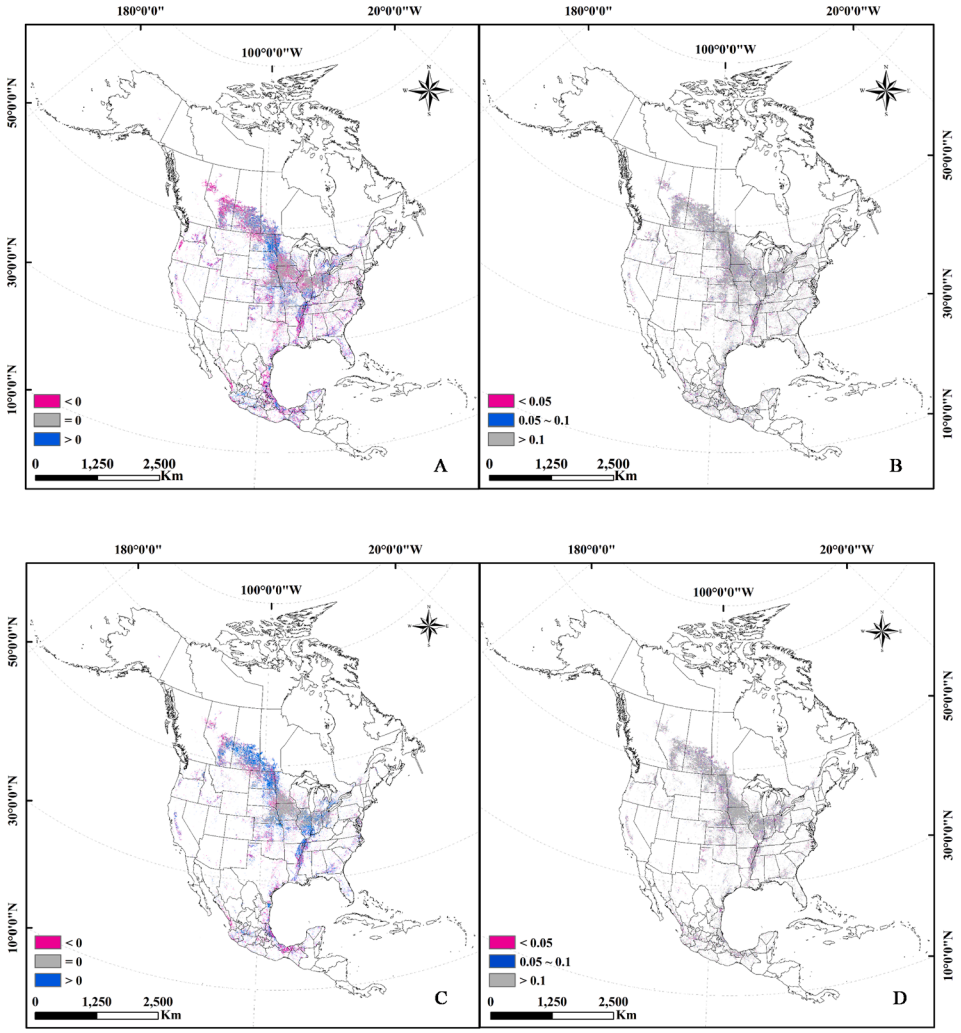

Fig. 5. Mean-Kendal trend tests for the planting (A: Slope, B: P values) and harvesting dates (C: Slope, D: P values) of the first growing season across North America (Slope: change rate of crop phenological dates; P values: the confidence of trend analysis; The slope values lying outside the 95% confidence intervals were not included in the statistics; pixels with less than 12 years being identified as cropland, which were not included in the Mann-Kendall statistical test).

v3.0, and the cropland areas fall within six of them. In this study, we regrouped two tropics into the region a, four subtropics into the region b, three temperate zones into the region c (Appendix Fig. S6). We excluded the year 2000 in the trend analysis because of the incomplete MODIS EVI time series. The analysis showed various temporal patterns in the crop growing season length among eco-regions in North America during the study period. Shortened crop growing seasons were mainly found in tropics (slope = −0.146, $P < 0.01$), while significantly extended crop growing seasons occurred over the subtropics (0.48 days/year) and temperate zones (0.65 days/year).

3.6.2. Correlations between crop phenology and climatic factors

Our climate analysis suggested that, at the continental scale, planting dates had a negative correlation with the average daily minimum/maximum temperatures during the crop sowing season (minimum temperature: r = −0.50, $p < 0.01$; maximum temperature: r = −0.62, $p < 0.01$). An increase of 1 °C in average daily minimum/maximum temperatures from April to June resulted in an advancement of 4.26/4.48 days in crop planting dates (Figs. 8 and 9). For the harvesting dates, our results suggested that an increase of 1 °C in minimum temperature during August through October resulted in a delay of 0.66 days (r = 0.10, $P < 0.01$); while an increase of 1 °C in maximum temperature during the same period resulted in an advancement of 2.22 days (r = −0.40, $P < 0.01$). Correlation analysis for the other three phenological stages (jointing, heading, and maturity dates) and climatic temperature can be found in Appendix Figs. S7 and S8. Over the study period, significant negative correlations were found between three crop stages (jointing, heading, and maturity dates) and average daily maximum temperature. Two of three stages (jointing and heading dates) showed advanced trends with the increasing average daily minimum temperature.

4. Discussion

4.1. Satellite-based crop phenology approach

Satellite imagery has been widely used for crop phenology monitoring over the past decades (Boschetti et al., 2009; Chmielewski et al., 2004; Hmimina et al., 2013). The NDVI is one of the vegetation indexes for extracting crop phenology. For example, You et al. (2013) used a threshold-based method and the AVHRR NDVI time series for identifying the start and end of the growing seasons for 43 different agricultural zones in China. Zheng et al. (2016a,b) produced a synthetic NDVI time series fused from SPOT 5 and MODIS to extract crop phenology over areas with high fragmented farmlands. However, the NDVI application is limited by its tendency to saturate at high canopy density and coverage (Bausch, 1993). When the crops reach canopy closure, the NDVI also tends to saturate (Rouse et al., 1974) and produce inaccurate

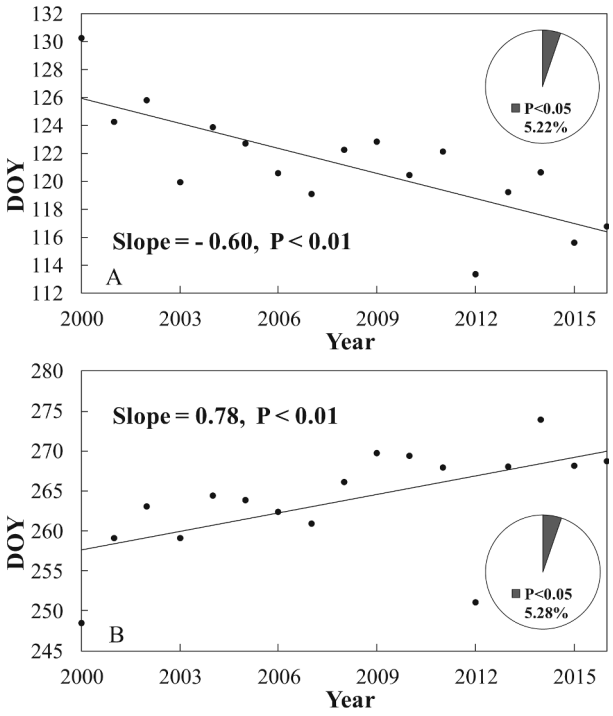

Fig. 6. Changing trend of averaged planting dates (A) and harvesting dates (B) in North America ($p < 0.05$) (pixels that were identified as cropland for less than 12 years were not included in the Mann-Kendall statistical test).

estimates of crop phenology, especially for crop heading date detection (Son et al., 2014). Also, the NDVI is very sensitive to soil background effects at incomplete vegetative cover conditions, which may bring more uncertainties in the early stage of crop growth when the LAI is still low (Huete, 1988). In contrast, EVI is constructed by decoupling the canopy background signal and reducing atmospheric influences, which can overcome the saturation and soil noise problems of NDVI (Huete et al., 1997). Using the smoothed EVI time series, Sakamoto et al. (2005) proposed the wavelet transform-based method to retrieve the rice planting, heading, and harvesting dates in Japan successfully. But the mother wavelet and the threshold used for determining each phenological stage vary with regions and crop species, limiting the method's application for other crops and over large areas.

Generally, remote-sensing-based approaches to detect plant phenology can be classified into two general categories, i.e., threshold-based methods and VI change detection methods (Zeng et al., 2020). Threshold-based methods use identical thresholds to determine crop phenological stages in all cropping systems. For example, Delbart et al. (2005) adopted 20% of the NDVI amplitude to estimate senescence dates of both croplands and natural vegetation types. White et al. (1997) used 50% of the NDVI amplitude to determine the start and end of the season. Threshold-based methods may generally describe changing patterns of crop phenology, but cannot catch discrepancies among various crops and different cropping systems (Huang et al., 2019). VI change detection methods retrieve the crop phenological dates through detecting the changing characteristics of the VI time series curve, such as some key points in the VI and the first derivative of VI or the changing rates of curvature (Zeng et al., 2020). VI change detection method was considered an effective way to extract the phenological metrics for general vegetation types. For example, Sakamoto et al. (2010) used a Two-step Filtering method to analyze the changing characteristics of VI curves and detect the specific phenological dates of corn and soybean in eastern Nebraska. However, changing characteristics derived from VI profile might be sensitive to non-vegetation-related variations such as noise components caused by aerosols and bidirectional reflectance distribution or other climatic factors, resulting in significant uncertainties in the phenology timing estimates. Besides, complicated crop planting patterns, such as double or multiple cropping systems, make the crop phenology detection more difficult over the large area (Ogle et al., 2005).

In this study, we combined the advantages of both threshold-based and VI change detection methods by using specific key points of EVI cures and its first/second derivatives, along with the dynamic thresholds to confine the ranges of each stage. We expanded to quantify five main crop phenological phases (i.e., the dates of planting, jointing, heading, maturity, and harvesting) of seven major crop types over North America during 2000–2016. Compared with the VI change detection method without setting thresholds, our improved approach showed better performances (Appendix Table S4). The estimated crop phenological stages also demonstrate a more favorable agreement with ground information than previous studies (Section 3.3).

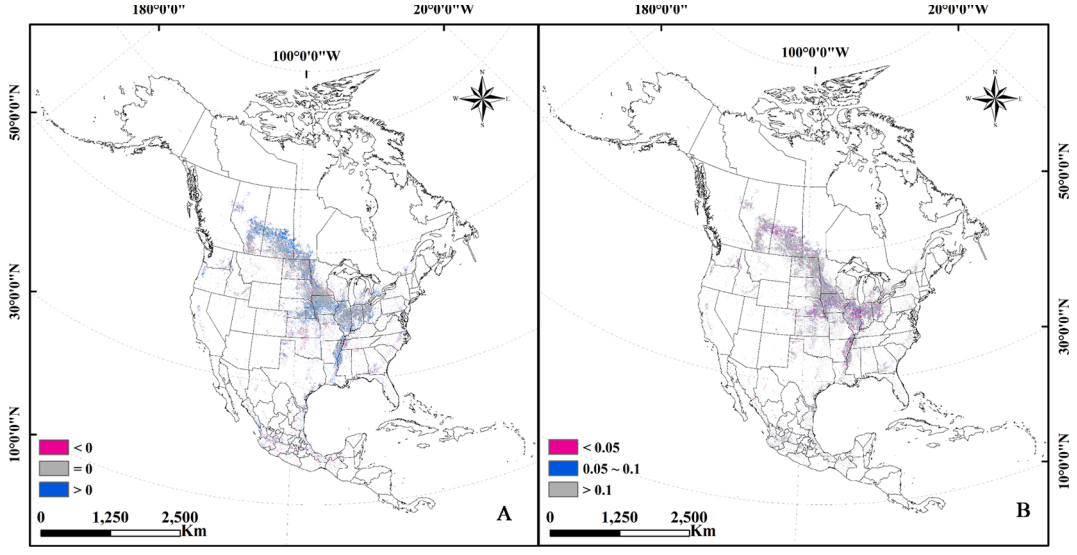

Fig. 7. Mean-Kendal trend tests for the crop growing season (A: Slope, B: P values) across North America (pixels identified as cropland for less than 12 years were not included in the Mann-Kendall statistical test).

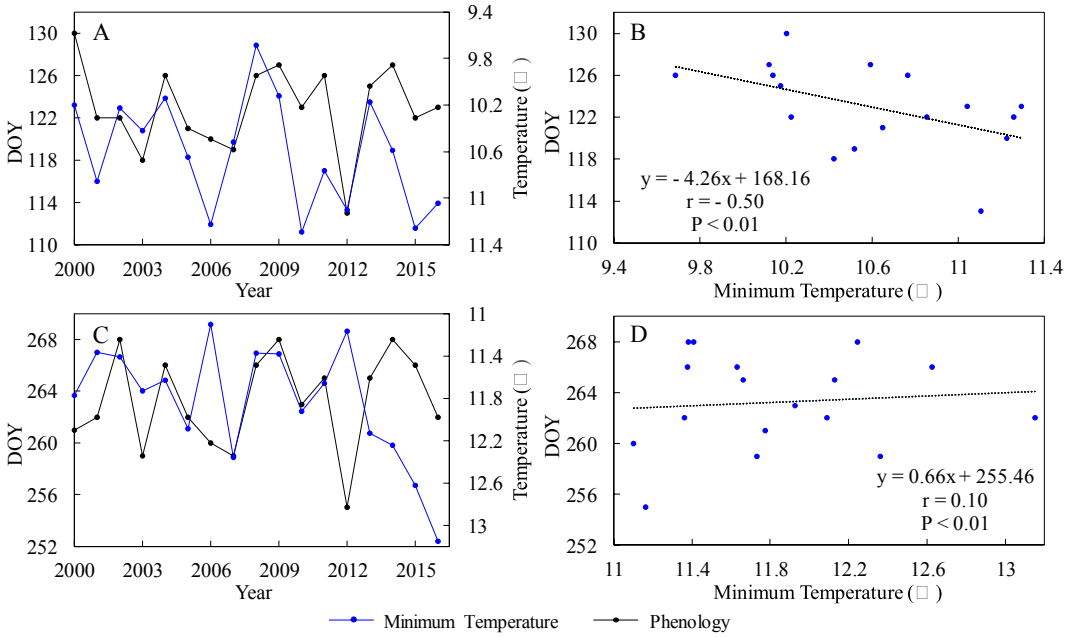

Fig. 8. Interannual changes in estimated planting and harvesting dates and average daily minimum temperatures for planting (A, B: April to June) and harvesting seasons (C, D: August to October) in North America during 2000–2016.

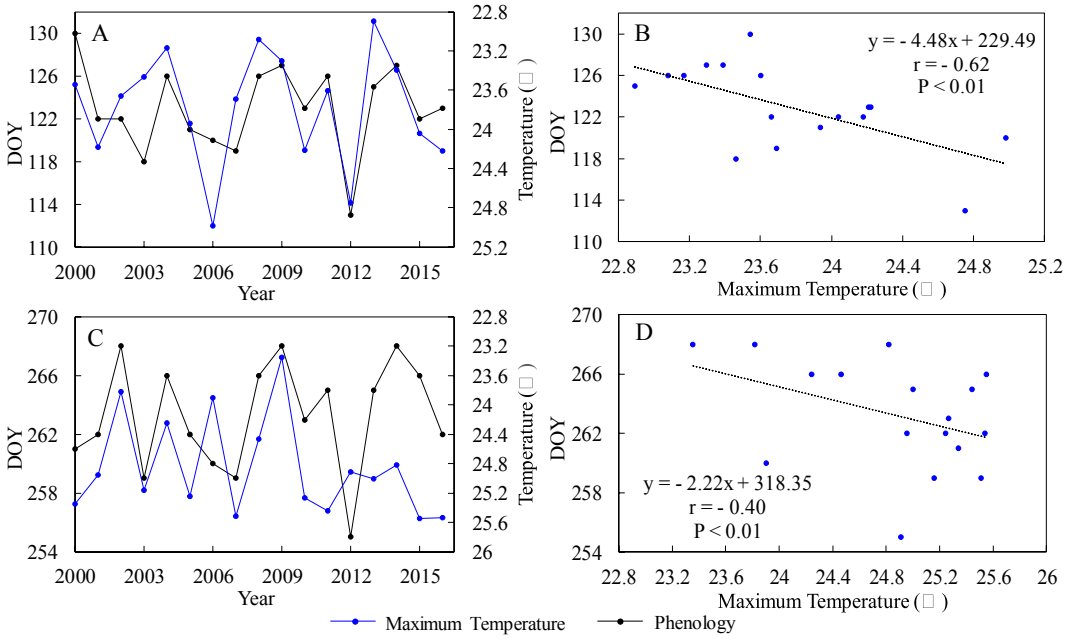

Fig. 9. Interannual changes in estimated planting and harvesting dates and average daily maximum temperatures for planting (A, B: April to June) and harvesting seasons (C, D: August to October) in North America during 2000–2016.

4.2. Changing trends in crop phenology

The temporal and spatial variations in crop phenology have been widely investigated in previous studies. Spatially, many studies indicated a latitude-dependent changing pattern in crop phenology, particularly in mid and high Northern Hemispheres (Chmielewski et al., 2004; Liu et al., 2017a,b; Luo et al., 2020; Yu et al., 2012). Our spatially explicit results confirmed these findings by showing a slightly increasing trend in planting and harvesting dates with latitudinal gradients from 20° to 70°N in North America (Fig. 4). Crop phenology in Mexico did not exhibit a latitudinally changing pattern. It might be partially attributed to the non-obvious latitudinal gradient of temperature in the tropical region (Ogle et al., 2005), different cropping systems (Hansen et al., 2016), and other factors related to management practices (Martin et al., 2005).

As for temporal variations, many studies have reported that some crop phenological stages, such as planting and harvest dates, had either delayed or advanced over recent decades. For example, an analysis of observations from phenological network stations showed earlier corn planting dates (0.17 days/year) in Germany from 1961 to 2000 (Chmielewski et al., 2004). Using long-term VI time series, Wang et al. (2017) observed an advance in spring green-up date for winter wheat (0.18 days/year) in North China Plain over the period 1982–2013. Sacks and Kucharik (2011) reported advanced planting trends (0.40 days/year

for corn and 0.50 days/year for soybean) in the U.S. during 1981–2005. Zhu et al. (2012) observed the delayed dormancy (0.55 days/year) during 1982–2006, with mean rates averaged by natural vegetation and crops in North America. These studies are limited to either specific crop types or phenological stages, with few at large scales and over long time series. In this study, we derived spatially explicit five crop phenological stages of seven crop types at the North America continental scale. Our estimated changes in planting and harvesting dates fall within the reasonable range compared to previous studies, despite slightly more apparent changing rates (Section 3.5, Fig. 6) due to different data sources and study periods. Our spatially explicit estimates of multiple phenological stages for seven major crops provide more detailed information for crop yield prediction and climate change assessments at large scales.

The length of growing season may have significant effects on seasonal variations in carbon, water, and nutrient processes, as well as land surface energy balance, therefore have implications for crop security and terrestrial biogeochemical cycles. Several studies have suggested the extended or shortened period for various crop types in different regions. For example, Chen et al. (2012) found that the growth durations of rice, corn, and soybean in Northeast China have prolonged by 14 days, 7.0 days, and 2.7 days since the 1950s, respectively. Sacks and Kucharik (2011) presented that the crop growth period in the U.S. has been longer by 0.50 days/year for corn and 0.31 days/year for soybean from 1981 to 2005. Our study also reported a prolonged crop growing season length, especially in the temperate and subtropical areas (Section 3.6.1, Fig. 7 and Appendix Fig. S6). Our extended crop growing period is well supported by some previous studies based on the intensive ground observations (Tao et al., 2014; Zhang et al., 2014) and regional estimations (Peltonen-Sainio et al., 2009). The concurrent of advanced planting and delayed harvesting contributes to the prolonged crop growing seasons in North America. The crop variety shift aiming to improve crop production may also extend the growing season (Tao et al., 2012; Wang et al., 2013, 2018). In addition, irrigation, intensive management practices such as reduced or zero-till, cover crop, and fertilizer use have been significantly improved during the last several decades, which may have positively affected crop phenology development (He et al., 2015).

4.3. Crop phenology in correlation with climate factors

Previous studies have indicated that climate changes have promoted variations in vegetation phenology (Oteros et al., 2015; Sacks et al., 2010; Sparks et al., 2005; Wang et al., 2016). Temperatures have been regarded as the primary control of vegetation phenological progress (Badeck et al., 2004; Piao et al., 2019). The distinct responses of crop phenology to temperatures in the spring or autumn season were reported in many studies (e.g., He et al., 2015; Kucharik, 2006; Tao et al., 2014; Zhang et al., 2019). Some studies found that temperature changes had led to appreciable responses in crop phenology in many parts of the Northern Hemisphere. For example, Tao et al. (2006) analyzed observations on agro-meteorological stations and found that the planting dates of corn were significantly related to the spring temperatures during 1981–2000, with an advance of 2.12 days and 2.28 days for each 1 °C rise in minimum and maximum temperatures, respectively. Chmielewski et al. (2004) showed that an increase of 1 °C in average temperatures between February and April led to an advanced beginning of the growing season of fruit trees and crops by 4.7 days in Germany from 1961 to 2000. Our study confirmed these findings and suggested that an increase of 1 °C in average daily minimum/maximum temperatures from April to June might have resulted in an advancement of 4.26–4.48 days in crop planting dates. Accordingly, an increase of 1 °C in average daily minimum/maximum temperature from August to October might have resulted in a delay of 0.66 days or advancement of 2.22 days in crop harvesting dates in North America during the study period.

Vegetation growth in the North Hemisphere mid-high latitudes is particularly sensitive to temperature changes in spring (Nemani et al., 2003; Slayback et al., 2003; Piao et al., 2019; Schwartz et al., 2006). This is consistent with our results, showing more evident changes in the planting dates than the harvesting dates in response to temperature changes. When investigating spatial patterns, our results displayed both advances and delays occurring across the crop areas (Fig. 5) in response to highly diverse climatic conditions. This finding agrees with Schwartz et al. (2006), which also found spatially heterogeneous of the start of season across North America.

4.4. Uncertainties and future needs

Our study involved mutiple datasets and a range of statistical approaches, which potentially introduced uncertainties to the estimated results. First, we only used the 2005 and 2010 land use and cover datasets because annual land cover maps were not available for entire North America; this might bring some uncertainties to identifying crop phenological stages. Second, the winter wheat is generally planted in late autumn and enters the dormant period before the next year; its EVI curves tend to show two peaks due to the over-wintering stages, which may result in biased identification of the planting dates. Third, we detected the harvesting date of the first season as the planting date of the second season. We acknowledge this scheme may not work for all situations and could be improved when more detailed phenology information for the double cropping system is available. Forth, the perennial grasses were included in the classification of cropland in this study; in this case, most parts of the forage grass with two harvest seasons were identified as double cropping systems, which might result in overestimation of the distribution of double crops. Moreover, the estimated crop phenological stages might have relatively higher uncertainties over areas with more fragmented croplands due to the effects of mixed and perimeter pixels at a 500 m spatial scale. In addition, the prolonged crop growing season might be overestimated because pasture or forage grass was difficult to separate from cropland in phenology identification at coarse spatial scales. In the next step, phenological dates of winter wheat crop should be included as more crop-specific distribution maps are available. Data fusion of high-resolution satellite imagery is needed for reducing uncertainties in fragmented areas where mixed cropland pixels are dominant. More ground observations and long-term time series crop-specific maps will booster the accuracy of crop phenology identification.

5. Conclusions

This study quantified spatiotemporal patterns in five phenological stages of seven crop types across North America from 2000 to 2016 based on the MODIS EVI time series data. The estimated cropping intensity and phenological stages agree favorably with those observed from field surveys, satellite-based maps, and results from other studies. Our results demonstrated that the improved approach is capable of realistically capturing changing patterns in crop phenology at large scales. This approach overcomes the overfitting flaws of the polynomial function at the start and end of the growing season. It can be applied to other regions where no substantial site-level field observations for parameterization and validation available. To the best of our knowledge, this study offers the first attempt to provide spatially-explicit time series information of five major crop phenological dates with a moderate spatial resolution at the continental scale. Our study sheds light on how the crop phenology spatially responded to climate change. The derived crop phenological datasets can be used to drive process-based crop or ecosystem models for large-scale crop yield prediction and biogeochemical dynamics assessment, and help to formulate climate-resilient development strategies.

Declaration of Competing Interest

The authors declare that they have no known competing financial interests or personal relationships that could have appeared to influence the work reported in this paper.

Acknowledgments

This work was supported by the National Institute of Food and Agriculture, U.S. Department of Agriculture (NIFA-USDA Hatch project 2352437000), and NASA Kentucky under NASA award (number NNX15AR69H). The work by L. Ji was performed under USGS Contract 140G0119C0001. Contributions by A.C. Ruane were supported by the NASA Earth Sciences Division support of the NASA GISS Climate Impacts Group. JBF contributed to this research at the Jet Propulsion Laboratory, California Institute of Technology, under a contract with the National Aeronautics and Space Administration. California Institute of Technology. Government sponsorship acknowledged. JBF was supported in part by NASA IDS, CMS, and INCA programs. We thank Dr. Sanath Sathyachandran for reviewing the manuscript and providing valuable comments. Datasets derived from this study will be made available on the website. The authors declare no conflicts of interest.

Any use of trade, firm, or product names is for descriptive purposes only and does not imply endorsement by the U.S. Government.

Appendix A. Supplementary material

Supplementary data to this article can be found online at https://doi.org/10.1016/j.isprsjprs.2020.10.005.

References

Atkinson, P.M., Jeganathan, C., Dash, J., Atzberger, C., 2012. Inter-comparison of four models for smoothing satellite sensor time-series data to estimate vegetation phenology. Remote Sens. Environ. 123, 400–417. https://doi.org/10.1016/j.rse.2012.04.001.

Badeck, F.W., Bondeau, A., Böttcher, K., Doktor, D., Lucht, W., Schaber, J., Sitch, S., 2004. Responses of spring phenology to climate change. New Phytol. 162, 295–309. https://doi.org/10.1111/j.1469-8137.2004.01059.x.

Bausch, W.C., 1993. Soil background effects on reflectance-based crop coefficients for corn. Remote Sens. Environ. 46 (2), 213–222. https://doi.org/10.1016/0034-4257(93)90096-G.

Boschetti, M., Stroppiana, D., Brivio, P.A., Bocchi, S., 2009. Multi-year monitoring of rice crop phenology through time series analysis of MODIS images. Int. J. Remote Sens. 30, 4643–4662. https://doi.org/10.1080/01431160802632249.

Borchers, A., Truex-Powell, E., Wallander, S., Nickerson, C., 2014. Multi-cropping practices: recent trends in double-cropping (No. 1476-2017-3888).

Cong, N., Piao, S., Chen, A., Wang, X., Lin, X., Chen, S., Han, S., Zhou, G., Zhang, X., 2012. Spring vegetation green-up date in China inferred from SPOT NDVI data: A multiple model analysis. Agric. For. Meteorol. 165, 104–113. https://doi.org/10.1016/j.agrformet.2012.06.009.

Congalton, R.G., 1991. A review of assessing the accuracy of classifications of remotely sensed data. Remote Sens. Environ. 37, 35–46. https://doi.org/10.1016/0034-4257(91)90048-B.

Chen, C., Qian, C., Deng, A., Zhang, W., 2012. Progressive and active adaptations of cropping system to climate change in Northeast China. Eur. J. Agron. 38, 94–103. https://doi.org/10.1016/j.eja.2011.07.003.

Chen, M., Griffis, T.J., Baker, J., Wood, J.D., Xiao, K., 2015. Simulating crop phenology in the Community Land Model and its impact on energy and carbon fluxes. J. Geophys. Res-Biogeo. 120 (2), 310–325. https://doi.org/10.1002/2014JG002780.

Chmielewski, F.-M., Müller, A., Bruns, E., 2004. Climate changes and trends in phenology of fruit trees and field crops in Germany, 1961–2000. Agric. For. Meteorol. 121, 69–78. https://doi.org/10.1016/S0168-1923(03)00161-8.

Delbart, N., Kergoat, L., Toan, T.L., Lhermitte, J., Picard, G., 2005. Determination of phenological dates in boreal regions using normalized difference water index. Remote Sens. Environ. 97, 26–38. https://doi.org/10.1016/j.rse.2005.03.011.

Diao, C., 2020. Remote sensing phenological monitoring framework to characterize corn and soybean physiological growing stages. Remote Sens. Environ. 248, 111960. https://doi.org/10.1016/j.rse.2020.111960.

FAO, 2016. FAOSTAT Land Use domain. http://www.fao.org/faostat/en/#data/RL. 2016.

Fitzgerald, R.W., Lees, B.G., 1994. Assessing the classification accuracy of multisource remote sensing data. Remote Sens. Environ. 47 (3), 362–368. https://doi.org/10.1016/0034-4257(94)90103-1.

Foody, G.M., Mathur, A., Sanchez-Hernandez, C., Boyd, D.S., 2006. Training set size requirements for the classification of a specific class. Remote Sens. Environ. 104, 1–14. https://doi.org/10.1016/j.rse.2006.03.004.

Gao, F., Anderson, M.C., Zhang, X., Yang, Z., Alfieri, J.G., Kustas, W.P., Prueger, J.H., 2017. Toward mapping crop progress at field scales through fusion of Landsat and MODIS imagery. Remote Sens. Environ. 9–25. https://doi.org/10.1016/j.rse.2016.11.004.

Gilbert, R.O., 1987. Statistical Methods for Environmental POLLUTION monitoring. John Wiley & Sons.

Gumma, M.K., Thenkabail, P.S., Maunahan, A., Islam, S., Nelson, A., 2014. Mapping seasonal rice cropland extent and area in the high cropping intensity environment of Bangladesh using MODIS 500m data for the year 2010. ISPRS J. Photogramm. 91, 98–113. https://doi.org/10.1016/j.isprsjprs.2014.02.007.

Hansen, N.C., Allen, B.L., Anapalli, S., Blackshaw, R.E., Lyon, D.J., Machado, S., 2016. Dryland agriculture in North America. In: Innovations in Dryland Agriculture. Springer, Cham, pp. 415–441. https://doi.org/10.1007/978-3-319-47928-6_15.

He, L., Asseng, S., Zhao, G., Wu, D.R., Yang, X.Y., Zhuang, W., et al., 2015. Impacts of recent climate warming, cultivar changes, and crop management on winter wheat phenology across the Loess Plateau of China. Agric. For. Meteorol. 200, 135–143. https://doi.org/10.1016/j.agrformet.2014.09.011.

Heggenstaller, A.H., Anex, R.P., Liebman, M., Sundberg, D.N., Gibson, L.R., 2008. Productivity and nutrient dynamics in bioenergy double-cropping systems. Agron. J. 100 (6), 1740–1748. https://doi.org/10.2134/agronj2008.0087.

Hmimina, G., Dufrêne, E., Pontailler, J.Y., Delpierre, N., Aubinet, M., Caquet, B., Gross, P., 2013. Evaluation of the potential of MODIS satellite data to predict vegetation phenology in different biomes: An investigation using ground-based NDVI measurements. Remote Sens. Environ. 132, 145–158. https://doi.org/10.1016/j.rse.2013.01.010.

Hodges, T., 1991. Temperature and water stress effects on phenology. Predict. Crop Phenol. 7–13.

Hubert-Moy, L., Cotonnec, A., Le Du, L., Chardin, A., Pérez, P., 2001. A comparison of parametric classification procedures of remotely sensed data applied on different landscape units. Remote Sens. Environ. 75, 174–187. https://doi.org/10.1016/S0034-4257(00)00165-6.

Huang, X., Liu, J., Zhu, W., Atzberger, C., Liu, Q., 2019. The optimal threshold and vegetation index time series for retrieving crop phenology based on a modified dynamic threshold method. Remote Sens. 11 (23), 2725. https://doi.org/10.3390/rs11232725.

Huete, A., Didan, K., Miura, T., Rodriguez, E.P., Gao, X., Ferreira, L.G., 2002. Overview of the radiometric and biophysical performance of the MODIS vegetation indices. Remote Sens. Environ. 83, 195–213. https://doi.org/10.1016/S0034-4257(02)00096-2.

Huete, A., 1988. Huete, AR A soil-adjusted vegetation index (SAVI). Remote Sensing of Environment. Remote Sens. Environ. 25, 295–309. http://hdl.handle.net/10453/13646.

Huete, A., Justice, C., Liu, H., 1994. Development of vegetation and soil indices for MODIS-EOS. Remote Sens. Environ. 49, 224–234. https://doi.org/10.1016/0034-4257(94)90018-3.

Huete, A., Justice, C., Van Leeuwen, W., 1999. MODIS vegetation index (MOD13). Algorithm Theoret. Basis Doc. 3 (213). https://modis.gsfc.nasa.gov/data/atbd/atbd_mod13.pdf.

Huete, A.R., Liu, H.Q., Batchily, K., van Leeuwen, W., 1997. A comparison of vegetation indices over a global set of TM images for EOS-MODIS. Remote Sens. Environ. 59 (3), 440–451. https://doi.org/10.1016/S0034-4257(96)00112-5.

Jiang, Z., Huete, A.R., Didan, K., Miura, T., 2008. Development of a two-band enhanced vegetation index without a blue band. Remote Sens. Environ. 112 (10), 3833–3845. https://doi.org/10.1016/j.rse.2008.06.006.

Jin, Z., Zhuang, Q., He, J.S., Luo, T., Shi, Y., 2013. Phenology shift from 1989 to 2008 on the Tibetan Plateau: an analysis with a process-based soil physical model and remote sensing data. Clim. Change 119 (2), 435–449. https://doi.org/10.1007/s10584-013-0722-7.

Kelley, K.W., Sweeney, D.W., 2005. Tillage and urea ammonium nitrate fertilizer rate and placement affects winter wheat following grain sorghum and soybean. J. Agron. 97 (3), 690–697. https://doi.org/10.2134/agronj2004.0156.

Kisi, O., Ay, M., 2014. Comparison of Mann-Kendall and innovative trend method for water quality parameters of the Kizilirmak River, Turkey. J. Hydrol. 513, 362–375. https://doi.org/10.1016/j.jhydrol.2014.03.005.

Kotsuki, S., Tanaka, K., 2015. SACRA – a method for the estimation of global high-resolution crop calendars from a satellite-sensed NDVI. Hydrol. Earth Syst. Sci. 19, 4441–4461. https://doi.org/10.5194/hess-19-4441-2015.

Kucharik, C.J., 2006. A multidecadal trend of earlier corn planting in the central USA. Agron. J. 98 (6), 1544–1550. https://doi.org/10.2134/agronj2006.0156.

Li, L., Friedl, M., Xin, Q., Gray, J., Pan, Y., Frolking, S., 2014. Mapping crop cycles in China using MODIS-EVI time series. Remote Sens. 6, 2473–2493. https://doi.org/10.3390/rs6032473.

Liu, L., Wang, E., Zhu, Y., Tang, L., Cao, W., 2013. Quantifying three-decade changes of single rice cultivars in China using crop modeling. Field Crops Res. 149, 84–94. https://doi.org/10.1016/j.fcr.2013.04.025.

Liu, L., Zhang, X., Yu, Y., Guo, W., 2017a. Real-time and short-term predictions of spring phenology in North America from VIIRS data. Remote Sens. Environ. 194, 89–99. https://doi.org/10.1016/j.rse.2017.03.009.

Liu, Q., Li, X., Liu, G., Huang, C., Guo, Y., 2016a. Cotton area and yield estimation at Zhanhua county of China using HJ-1 EVI time series. In: ITM Web of Conferences: EDP Sciences, p. 09001. https://doi.org/10.1051/itmconf/20160709001.

Liu, Q., Fu, Y., Zhu, Z., Liu, Y., Liu, Z., Huang, M., et al., 2016b. Delayed autumn phenology in the Northern Hemisphere is related to change in both climate and

spring phenology. Glob. Change Biol. 22, 3702–3711. https://doi.org/10.1111/gcb.13311.
Liu, Z., Wu, C., Liu, Y., Wang, X., Fang, B., Yuan, W., Ge, Q., 2017b. Spring green-up date derived from GIMMS3g and SPOT-VGT NDVI of winter wheat cropland in the North China Plain. ISPRS J. Photogramm. 130, 81–91. https://doi.org/10.1016/j.isprsjprs.2017.05.015.
Lobell, D.B., Ortiz-Monasterio, J.I., Sibley, A.M., Sohu, V.S., 2013. Satellite detection of earlier wheat sowing in India and implications for yield trends. Agric. Syst. 115, 137–143. https://doi.org/10.1016/j.agsy.2012.09.003.
Lu, L., Wang, C., Guo, H., Li, Q., 2013. Detecting winter wheat phenology with SPOT-VEGETATION data in the North China Plain. Geocarto. Int. 29, 244–255. https://doi.org/10.1080/10106049.2012.760004.
Luo, Y., Zhang, Z., Chen, Y., Li, Z., Tao, F., 2020. ChinaCropPhen1km: a high-resolution crop phenological dataset for three staple crops in China during 2000–2015 based on leaf area index (LAI) products. Earth Syst. Sci. Data 12 (1). https://doi.org/10.5194/essd-12-197-2020.
Marra, M.C., Carlson, G.A., 1986. Double-cropping wheat and soybeans in the southeast.
Martin, K.E.A., Hodgen, P.J., Freeman, K.W., Melchiori, R., Arnall, D.B., Teal, R.K., Stone, M.L., 2005. Plant-to-plant variability in corn production. J. Agron. 97 (6), 1603–1611. https://doi.org/10.2134/agronj2005.0129.
Menenti, M., Azzali, S., Verhoef, W., Van Swol, R., 1993. Mapping agro-ecological zones and time lag in vegetation growth by means of Fourier analysis of time series of NDVI images. Adv. Space Res. 13 (5), 233–237. https://doi.org/10.1016/0273-1177(93)90550-U.
Mercier, A., Betbeder, J., Baudry, J., Le Roux, V., Spicher, F., Lacoux, J., Hubert-Moy, L., 2020. Evaluation of Sentinel-1 & 2 time series for predicting wheat and rapeseed phenological stages. ISPRS J. Photogramm. 163, 231–256. https://doi.org/10.1016/j.isprsjprs.2020.03.009.
Næsset, E., 1996. Conditional tau coefficient for assessment of producer's accuracy of classified remotely sensed data. ISPRS J. Photogramm. 51 (2), 91–98. https://doi.org/10.1016/0924-2716(69)00007-4.
Nemani, R.R., Keeling, C.D., Hashimoto, H., Jolly, W.M., Piper, S.C., Tucker, C.J., Running, S.W., 2003. Climate-driven increases in global terrestrial net primary production from 1982 to 1999. Science 300 (5625), 1560–1563. https://doi.org/10.1126/science.1082750.
Ogle, S.M., Breidt, F.J., Paustian, K., 2005. Agricultural management impacts on soil organic carbon storage under moist and dry climatic conditions of temperate and tropical regions. Biogeochemistry 72, 87–121. https://doi.org/10.1007/s10533-004-0360-2.
Ortiz-Monasterio, J.I., Lobell, D.B., 2007. Remote sensing assessment of regional yield losses due to sub-optimal planting dates and fallow period weed management. Field Crop Res. 101, 80–87. https://doi.org/10.1016/j.fcr.2006.09.012.
Oteros, J., Garcia-Mozo, H., Botey, R., Mestre, A., Galan, C., 2015. Variations in cereal crop phenology in Spain over the last twenty-six years (1986–2012). Clim. Change 130, 545–558. https://doi.org/10.1007/s10584-015-1363-9.
Pan, Z., Huang, J., Zhou, Q., Wang, L., Cheng, Y., Zhang, H., et al., 2015. Mapping crop phenology using NDVI time-series derived from HJ-1 A/B data. Int. J. Appl. Earth Obs. 34, 188–197. https://doi.org/10.1016/j.jag.2014.08.011.
Peltonen-Sainio, P., Jauhiainen, L., Hakala, K., Ojanen, H., 2009. Climate change and prolongation of growing season: changes in regional potential for field crop production in Finland. Agric. Food Sci. http://urn.fi/URN:NBN:fi-fe2015090311189.
Piao, S., Fang, J., Zhou, L., Ciais, P., Zhu, B., 2006. Variations in satellite-derived phenology in China's temperate vegetation. Glob. Change Biol. 12 (4), 672–685. https://doi.org/10.1038/nature06444.
Piao, S., Liu, Q., Chen, A., Janssens, I.A., Fu, Y., Dai, J., et al., 2019. Plant phenology and global climate change: current progresses and challenges. Glob. Change Biol. 25 (6), 1922–1940. https://doi.org/10.1111/gcb.14619.
Portmann, F.T., Siebert, S., Döll, P., 2010. MIRCA2000—Global monthly irrigated and rainfed crop areas around the year 2000: A new high-resolution data set for agricultural and hydrological modeling. Glob. Biogeochem. Cycl. 24 (1), GB1011. https://doi.org/10.1029/2008GB003435.
R Development Core Team, https://www.R-project.org/. 2011.
Reed, B.C., 2013. Trend analysis of time-series phenology of North America derived from satellite data. Gisci. Remote Sens. 43, 24–38. https://doi.org/10.2747/1548-1603.43.1.24.
Ren, J., Chen, Z., Zhou, Q., Tang, H., 2008. Regional yield estimation for winter wheat with MODIS-NDVI data in Shandong, China. Int. J. Appl. Earth Obs. 10, 403–413. https://doi.org/10.1016/j.jag.2007.11.003.
Roerink, G., Menenti, M., Verhoef, W., 2000. Reconstructing cloudfree NDVI composites using Fourier analysis of time series. Int. J. Remote Sens. 21, 1911–1917. https://doi.org/10.1080/014311600209814.
Rouse, J.W., Hass, R.H., Schell, J.A., Deering, D.W., 1974. Monitoring vegetation systems in the Great Plains with ERTS. In: The 3rd Earth Resources Technology Satellite-1 Symposium, Greenbelt, MD, pp. 309–317.
Sacks, W.J., Deryng, D., Foley, J.A., Ramankutty, N., 2010. Crop planting dates: an analysis of global patterns. Glob. Ecol. Biogeogr. 19, 607–620. https://doi.org/10.1111/j.1466-8238.2010.00551.x.
Sacks, W.J., Kucharik, C.J., 2011. Crop management and phenology trends in the U.S. Corn Belt: Impacts on yields, evapotranspiration and energy balance. Agric. For. Meteorol. 151, 882–894. https://doi.org/10.1016/j.agrformet.2011.02.010.
Sakamoto, T., Yokozawa, M., Toritani, H., Shibayama, M., Ishitsuka, N., Ohno, H., 2005. A crop phenology detection method using time-series MODIS data. Remote Sens. Environ. 96, 366–374. https://doi.org/10.1016/j.rse.2005.03.008.
Sakamoto, T., Van Nguyen, N., Ohno, H., Ishitsuka, N., Yokozawa, M., 2006. Spatio–temporal distribution of rice phenology and cropping systems in the Mekong Delta with special reference to the seasonal water flow of the Mekong and Bassac rivers. Remote Sens. Environ. 100 (1), 1–16. https://doi.org/10.1016/j.rse.2005.09.007.
Sakamoto, T., 2018. Refined shape model fitting methods for detecting various types of phenological information on major US crops. ISPRS J. Photogramm. 138, 176–192. https://doi.org/10.1016/j.isprsjprs.2018.02.011.
Sakamoto, T., Wardlow, B.D., Gitelson, A.A., Verma, S.B., Suyker, A.E., Arkebauer, T.J., 2010. A two-step filtering approach for detecting maize and soybean phenology with time-series MODIS data. Remote Sens. Environ. 114, 2146–2159. https://doi.org/10.1016/j.rse.2010.04.019.
Schwartz, M.D., Ahas, R., Aasa, A., 2006. Onset of spring starting earlier across the Northern Hemisphere. Glob. Change Biol. 12, 343–351. https://doi.org/10.1111/j.1365-2486.2005.01097.x.
Sen, P.K., 1968. Estimates of the regression coefficient based on Kendall's tau. J. Am. Stat. Assoc. 63, 1379–1389. https://www.jstor.org/stable/2285891.
Slayback, D.A., Pinzon, J.E., Los, S.O., Tucker, C.J., 2003. Northern hemisphere photosynthetic trends 1982–99. Glob. Change Biol. 9 (1), 1–15. https://doi.org/10.1046/j.1365-2486.2003.00507.x.
Son, N.T., Chen, C.F., Chen, C.R., Duc, H.N., Chang, L.Y., 2014. A phenology-based classification of time-series MODIS data for rice crop monitoring in Mekong Delta, Vietnam. Remote Sens. 6 (1), 135–156. https://doi.org/10.3390/rs6010135.
Sparks, T., Croxton, P., Collinson, N., Taylor, P.W., 2005. Examples of phenological change, past and present, in UK farming. Ann. Appl. Biol. 146, 531–537. https://doi.org/10.1111/j.1744-7348.2005.050016.x.
Tao, F., Yokozawa, M., Xu, Y., Hayashi, Y., Zhang, Z., 2006. Climate changes and trends in phenology and yields of field crops in China, 1981–2000. Agric. For. Meteorol. 138, 82–92. https://doi.org/10.1016/j.agrformet.2006.03.014.
Tao, F., Zhang, S., Zhang, Z., 2012. Spatiotemporal changes of wheat phenology in China under the effects of temperature, day length and cultivar thermal characteristics. Eur. J. Agron. 43, 201–212. https://doi.org/10.1016/j.eja.2012.07.005.
Tao, F., Zhang, S., Zhang, Z., Rotter, R.P., 2014. Maize growing duration was prolonged across China in the past three decades under the combined effects of temperature, agronomic anagement, and cultivar shift. Glob. Change Biol. 20, 3686–3699. https://doi.org/10.1111/gcb.12684.
Taylor, R.D., Won, W.K., 2015. Outlook of the US and World Corn and Soybean Industries. 2015–2024.
Thompson, J.A., Paull, D.J., 2017. Assessing spatial and temporal patterns in land surface phenology for the Australian Alps (2000–2014). Remote Sens. Environ. 199, 1–13. https://doi.org/10.1016/j.rse.2017.06.032.
Thornton, M., Thornton, P., Wei, Y., Vose, R., Boyer, A., 2017. Daymet: Daily Surface Weather Data on a 1-km Grid for North America, Version 3. ORNL DAAC, Oak Ridge, Tennessee, USA.
Tveito, O.E., Bjørdal, I., Skjelvåg, A.O., Aune, B., 2005. A GIS-based agro-ecological decision system based on gridded climatology. Meteorol. Appl. 12 (1), 57–68. https://doi.org/10.1017/S1350482705001490.
Wang, J., Wang, E.L., Feng, L.P., Yin, H., Yu, W.D., 2013. Phenological trends of winter wheat in response to varietal and temperature changes in the North China Plain. Field Crops Res. 144, 135–144. https://doi.org/10.1016/j.fcr.2012.12.020.
Wang, S., Mo, X., Liu, Z., Baig, M.H.A., Chi, W., 2017. Understanding long-term (1982–2013) patterns and trends in winter wheat spring green-up date over the North China Plain. Int. J. Appl. Earth Obs. 57, 235–244. https://doi.org/10.1016/j.jag.2017.01.008.
Wang, Z., Chen, J., Li, Y., Li, C., Zhang, L., Chen, F., 2016. Effects of climate change and cultivar on summer maize phenology. Int. J. Plant. Prod. 10, 509–525. https://doi.org/10.22069/IJPP.2016.3046.
Wang, Z.B., Chen, J., Tong, W.J., Xu, C.C., Chen, F., 2018. Impacts of climate change and varietal replacement on winter wheat phenology in the north China Plain. Int. J. Plant Prod. https://doi.org/10.1007/s42106-018-0024-0.
White, K., Pontius, J., Schaberg, P., 2014. Remote sensing of spring phenology in northeastern forests: A comparison of methods, field metrics and sources of uncertainty. Remote Sens. Environ. 148, 97–107. https://doi.org/10.1016/j.rse.2014.03.017.
White, M.A., de Beurs, K.M., Didan, K., Inouye, D.W., Richardson, A.D., Jensen, O.P., et al., 2009. Intercomparison, interpretation, and assessment of spring phenology in North America estimated from remote sensing for 1982–2006. Glob. Change Biol. 15, 2335–2359. https://doi.org/10.1111/j.1365-2486.2009.01910.x.
White, M.A., Thornton, P.E., Running, S.W., 1997. A continental phenology model for monitoring vegetation responses to interannual climatic variability. Glob. Biogeochem. Cycl. 11, 217–234. https://doi.org/10.1029/97GB00330.
Wu, W.B., Peng, Y., Tang, H.J., Zhou, Q.B., Chen, Z.X., Shibasaki, R., 2010. Characterizing spatial patterns of phenology in cropland of China based on remotely sensed data. Agric. Sci. China 9 (1), 101–112. https://doi.org/10.1016/S1671-2927(09)60073-0.
Xin, J., Yu, Z., Louise, V.L., Paul, M.D., 2002. Mapping crop key phenological stages in the North China Plain using NOAA time series images. Int. J. Appl. Earth Obs. 4, 109–117. https://doi.org/10.1016/S0303-2434(02)00007-7.
Xu, X., Conrad, C., Doktor, D., 2017. Optimising phenological metrics extraction for different crop types in Germany using the moderate resolution imaging spectrometer (MODIS). Remote Sens. 9, 254. https://doi.org/10.3390/rs9030254.
Yan, H., Liu, F., Qin, Y., Niu, Z., Doughty, R., Xiao, X., 2019. Tracking the spatio-temporal change of cropping intensity in China during 2000–2015. Environ. Res. Lett. 14 (3) https://doi.org/10.1088/1748-9326/aaf9c7.
Yan, H., Xiao, X., Huang, H., Liu, J., Chen, J., Bai, X., 2014. Multiple cropping intensity in China derived from agro-meteorological observations and MODIS data. Chin. Geogr. Sci. 24, 205–219. https://doi.org/10.1007/s11769-013-0637-2.

You, L., Wood, S., Wood-Sichra, U., Wu, W., 2014. Generating global crop distribution maps: From census to grid. Agric. Syst. 127, 53–60. https://doi.org/10.1016/j.agsy.2014.01.002.

You, X., Meng, J., Zhang, M., Dong, T., 2013. Remote sensing based detection of crop phenology for agricultural zones in China using a new threshold method. Remote Sens. 5 (7), 3190–3211. https://doi.org/10.3390/rs5073190.

Yu, Y.Q., Huang, Y., Zhang, W., 2012. Changes in rice yields in China since 1980 associated with cultivar improvement, climate and crop management. Field Crop Res. 136, 65–75. https://doi.org/10.1016/j.fcr.2012.07.021.

Zeng, L., Wardlow, B., Wang, R., Shan, J., Tadesse, T., Hayes, M., Li, D., 2016. A hybrid approach for detecting corn and soybean phenology with time-series MODIS data. Remote Sens. Environ. 181, 237–250. https://doi.org/10.1016/j.rse.2016.03.039.

Zeng, L., Wardlow, B.D., Xiang, D., Hu, S., Li, D., 2020. A review of vegetation phenological metrics extraction using time-series, multispectral satellite data. Remote Sens. Environ. 237, 111511. https://doi.org/10.1016/j.rse.2019.111511.

Zhang, G., Xiao, X., Dong, J., Kou, W., Jin, C., Qin, Y., et al., 2015. Mapping paddy rice planting areas through time series analysis of MODIS land surface temperature and vegetation index data. ISPRS J. Photogramm. 106, 157–171. https://doi.org/10.1016/j.isprsjprs.2015.05.011.

Zhang, S., Tao, F.L., Zhang, Z., 2014. Rice reproductive growth duration increased despite of negative impacts of climate warming across China during 1981–2009. Eur. J. Agron. 54, 70–83. https://doi.org/10.1016/j.eja.2013.12.001.

Zhang, X., Friedl, M.A., Schaaf, C.B., Strahler, A.H., Hodges, J.C.F., Gao, F., Reed, B.C., Huete, A., 2003. Monitoring vegetation phenology using MODIS. Remote Sens. Environ. 84, 471–475. https://doi.org/10.1016/S0034-4257(02)00135-9.

Zhang, X., Liu, L., Henebry, G., 2019. Impacts of land cover and land use change on long-term trend of land surface phenology: a case study in agricultural ecosystems. Environ. Res. Lett. 14, 12. https://doi.org/10.1088/1748-9326/ab04d2.

Zhang, X., Wang, J., Henebry, G.M., Gao, F., 2020. Development and evaluation of a new algorithm for detecting 30 m land surface phenology from VIIRS and HLS time series ISPRS. J. Photogramm. 161, 37–51. https://doi.org/10.1016/j.isprsjprs.2020.01.012.

Zheng, H., Cheng, T., Yao, X., Deng, X., Tian, Y., Cao, W., Zhu, Y., 2016a. Detection of rice phenology through time series analysis of ground-based spectral index data. Field Crop Res. 198, 131–139. https://doi.org/10.1016/j.fcr.2016.08.027.

Zheng, Y., Wu, B., Zhang, M., Zeng, H., 2016b. Crop phenology detection using high spatio-temporal resolution data fused from SPOT5 and MODIS products. Sensors 16. https://doi.org/10.3390/s16122099.

Zhou, J., Jia, L., Menenti, M., 2015. Reconstruction of global MODIS NDVI time series: Performance of Harmonic ANalysis of Time Series (HANTS). Remote Sens. Environ. 163, 217–228. https://doi.org/10.1016/j.rse.2015.03.018.

Zhu, W., Tian, H., Xu, X., Pan, Y., Chen, G., Lin, W., 2012. Extension of the growing season due to delayed autumn over mid and high latitudes in North America during 1982–2006. Glob. Ecol. Biogeogr. 21, 260–271. https://doi.org/10.1111/j.1466-8238.2011.00675.